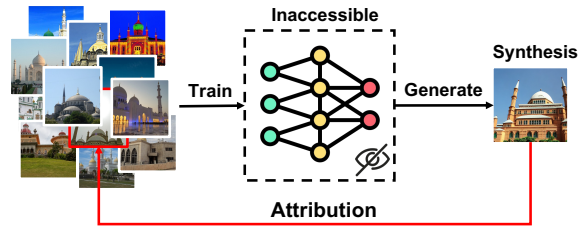


# Unsupervised Synthetic Image Attribution: Alignment and Disentanglement

Zongfang Liu <sup>\*1</sup> Guangyi Chen <sup>\*2 1</sup> Boyang Sun <sup>1</sup> Tongliang Liu <sup>3 1</sup> Kun Zhang <sup>2 1</sup>

## Abstract

As the quality of synthetic images improves, identifying the underlying concepts of model-generated images is becoming increasingly crucial for copyright protection and ensuring model transparency. Existing methods achieve this attribution goal by training models using annotated pairs of synthetic images and their original training sources. However, obtaining such paired supervision is challenging, as it requires either well-designed synthetic concepts or precise annotations from millions of training sources. To eliminate the need for costly paired annotations, in this paper, we explore the possibility of unsupervised synthetic image attribution. We propose a simple yet effective unsupervised method called Alignment and Disentanglement. Specifically, we begin by performing basic concept alignment using contrastive self-supervised learning. Next, we enhance the model's attribution ability by promoting representation disentanglement with the Infomax loss. This approach is motivated by an interesting observation: contrastive self-supervised models, such as MoCo and DINO, inherently exhibit the ability to perform simple cross-domain alignment. By formulating this observation as a theoretical assumption on cross-covariance, we provide a theoretical explanation of how alignment and disentanglement can approximate the concept-matching process through a decomposition of the canonical correlation analysis objective. On the real-world benchmarks, AbC, we show that our unsupervised method surprisingly outperforms the supervised methods. As a starting point, we expect our intuitive insights and experimental findings to provide a fresh perspective on this challenging task.



**Figure 1. Synthetic image attribution without model access.** Modern generative models are often closed-source and trained on vast datasets, making it challenging to attribute a generated image to its true training exemplar(s) when the model is inaccessible.

## 1. Introduction

Generative models are capable of producing high-quality synthetic images distinct from those in their training sets by merging elements from various images to create new scenes. Given the complexities and necessities of copyright and ownership, the attribution of synthetic images is critical. This process requires a deep understanding of the connections between the training data and the outputs generated by the model. It is essential to ensure that original content creators are properly recognized and compensated, address legal and ethical issues, aid in the detection of data leaks, and trace the origins of content.

Despite its importance, the task of data attribution remains a significant challenge and an open issue within the community, particularly for large-scale generative models. One promising method is to analyze the individual effects of each training sample. For instance, influence functions (Law, 1986; Huber & Ronchetti, 2011; Koh & Liang, 2017) are employed to assess the impact of specific training examples on a model's predictions, identifying the most influential data points. Similarly, Shapley value estimators (Feldman & Zhang, 2020) distribute credit to each data point based on its contribution to the model's overall performance. However, these methods struggle to scale up to the demands of current generative models (Ramesh et al., 2022; Saharia et al., 2022; Rombach et al., 2022), which involve training with millions or even billions of images. Recently, TRAK (Park et al., 2023) introduced a kernel machine-based approximation that enables faster attribution scoring in a surrogate space. Subsequent work adapted these ideas to diffusion models, including D-TRAK (Zheng et al., 2023) and Journey-TRAK (Georgiev et al., 2023), as well as more

<sup>\*</sup>Equal contribution <sup>1</sup>Mohamed bin Zayed University of Artificial Intelligence <sup>2</sup>Carnegie Mellon University <sup>3</sup>The University of Sydney. Correspondence to: Kun Zhang <kunz1@cmu.edu>.

direct diffusion-specific formulations (Młodożeniec et al., 2024; Lin et al., 2024). In parallel, recent efforts have also started to target text-to-image settings and improve practical efficiency (Wang et al., 2025). Despite this progress, scaling attribution to modern generative models remains difficult. Beyond sheer dataset and model size, many existing methods still presuppose access to model internals or training-time artifacts (e.g., parameters, gradients, checkpoints, or logs), which is often unrealistic for proprietary or closed-source deployments. This has motivated emerging directions that reduce reliance on such access, including model-agnostic or data-only formulations tailored to diffusion models (Zhao et al., 2025).

Another potential approach involves learning a latent representation space to align the concepts of synthetic images with their original training images. However, existing methods (Wang et al., 2023) for learning such a latent space typically require paired data for supervision. Obtaining this paired supervision is non-trivial; it requires either the creation of well-designed, customized synthetic concepts (Wang et al., 2023) or the extraction of ground-truth training samples from millions of potential sources (Feldman & Zhang, 2020). This computationally intensive annotation process exhibits limited generalization capabilities, and motivates us to think about the following important yet unresolved question:

*Is it possible to learn the concept matching space without paired annotation for synthetic image attribution?*

In this paper, we explore this question and propose a method, called Alignment and Disentanglement. During the Alignment phase, we apply a contrastive self-supervised learning method to achieve basic concept alignment by a shared mapping, targeting a latent space that allows comparison between synthetic and original training images. This method is inspired by experimental findings that demonstrate the inherent capability of models like MOCO (He et al., 2020) and DINO (Caron et al., 2021) to achieve cross-domain alignment. In the Disentanglement phase, we aim to further bridge the domain gap using Independent Component Analysis (ICA). Specifically, we learn two domain-specific models utilizing the Infomax loss (Bell & Sejnowski, 1995) to ensure that the latent variables are distributed within the same component-independent multivariate distribution. However, the independent ICA optimizations on two domains may cause permutations of the latent variables. To address these issues, we introduce a regularization term along with identity initialization for the mapping matrix to penalize potential permutations.

Given that the task of matching concepts across synthetic and original domains aligns with a canonical correlation analysis (CCA) framework (Hotelling, 1992), we provide

a theoretical explanation of how our method approximates this concept-matching process by decomposing the CCA targets. We discovered that the processes of alignment and disentanglement effectively serve as trivial solutions for CCA, optimizing across and within domains, respectively. In our experiments, we evaluate our methods using AbC (Wang et al., 2023), a large-scale benchmark renowned for its customized concept generation for synthetic image attribution. Our Alignment and Disentanglement method effectively eliminates the need for paired data and achieves performance comparable to, and at times even surpassing, that of supervised methods.

Our contributions are summarized as follows:

- We introduce a new unsupervised framework for synthetic image attribution that incorporates alignment and disentanglement.
- We provide a theoretical foundation for our unsupervised framework through the lens of CCA.
- We evaluate our framework on AbC, a large-scale benchmark with >4M images spanning object and style concepts, and report results on four test datasets covering both in-distribution and out-of-distribution settings; our method achieves performance comparable to supervised approaches even without paired data.

## 2. Related Work

### 2.1. Data Attribution

Currently, the majority of research on data attribution problems is based on influence analysis methods, which involve quantifying the impact of individual data points on the predictions of a machine learning model, helping to understand how specific examples affect model behavior and performance. Retraining-based influence analysis methods (Ghorbani & Zou, 2019; Jia et al., 2019; 2021; Kwon & Zou, 2021; Kandpal et al., 2022) directly measure how the inclusion or exclusion of specific data points affects the model’s performance. Gradient-based influence analysis methods (Sharchilev et al., 2018; Koh et al., 2019; Schioppa et al., 2022; Park et al., 2023) estimate influence by analyzing the gradients of the loss function with respect to the model parameters. Based on similar paradigms, recent works (Dai & Gifford, 2023; Zheng et al., 2023; Georgiev et al., 2023; Wang et al., 2024; Młodożeniec et al., 2024; Lin et al., 2024) provide solutions for data attribution in diffusion models. While effective, many influence-based methods require training-time access or model internals, which is often unavailable in practice; recent work improves efficiency for text-to-image attribution (Wang et al., 2025) and explores more model-agnostic/data-only formulations for diffusion models (Zhao et al., 2025). (Wang et al., 2023) provides a supervised method that considers the data attribution problem for generative models as an image retrieval

task. Though their method is practical because it does not require access to the generative model, it relies on paired synthetic-exemplar data, which is resource-intensive to acquire. To mitigate this issue, we aim to learn an attribution latent space without relying on paired annotations.

## 2.2. Canonical Correlation Analysis

In the supervised learning paradigm, learning the latent space to match the data from two different views can be formulated as Canonical Correlation Analysis (CCA) (Hotelling, 1992; Bach & Jordan, 2005), which finds the maximum projection for two sets of random vectors. It can be viewed as finding the shared latent variables from the observation in different generation function, as shown in the probabilistic interpretation (Bach & Jordan, 2005). Methods like (Bach & Jordan, 2002; Michaeli et al., 2016; Lindenbaum et al., 2020) extend CCA to the non-linear case by the kernel trick. Deep CCA (Andrew et al., 2013) and some following work (Lu et al., 2015; Wang et al., 2015) use neural networks to learn the non-parametric nonlinear mapping. While CCA is inherently well-suited for cross-domain alignment, traditional CCA methods rely on paired data, limiting their applicability in scenarios where paired data is infeasible. Building on (Bach & Jordan, 2005) our work offers a theoretical analysis and provides a potential solution to enable CCA without paired data.

## 2.3. Disentanglement Representation Learning

Unsupervised (self-supervised) representation learning (Radford et al., 2021; Caron et al., 2021; Chen et al., 2020b; He et al., 2020; Tian et al., 2020; Misra & Maaten, 2020) has shown considerable success in developing powerful and generalizable representations, but often lacks explainability. To enhance explainability and model controllability, methods have been developed to disentangle these representations (Chen et al., 2018; Zheng & Sun, 2019; Burgess et al., 2018; Denton et al., 2017; Higgins et al., 2018; Lee et al., 2018). Within these methods, those based on Independent Component Analysis (ICA) demonstrate strong identifiability properties for latent representations with better theoretical disentanglement guarantees. In the early stage, linear ICA (Comon, 1994; Bell & Sejnowski, 1995; Hyvärinen et al., 2001) requires assuming the non-Gaussian latent distribution. One of the widely used methods to achieve linear ICA is InfoMax loss (Bell & Sejnowski, 1995), which is applied in our implementation due to its flexibility. Recently, nonlinear ICA (Hyvärinen et al., 2019; Sorrenson et al., 2020; Hälvä & Hyvärinen, 2020; Lachapelle et al., 2022) have obtained robust theoretical results supporting the identifiability of latent variables, and enabled the use of deep neural networks such as VAE (Kingma, 2013) to address complex scenarios.

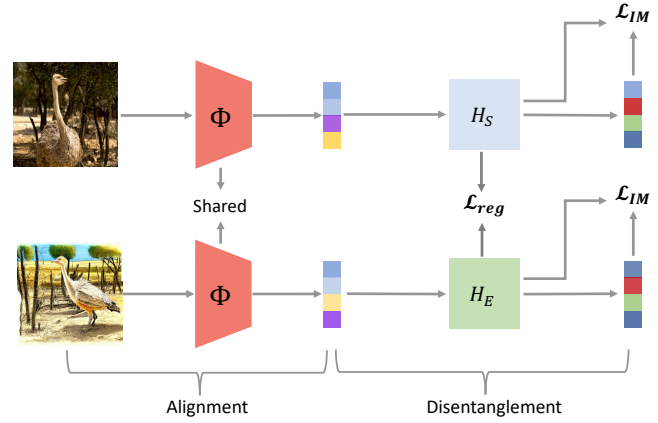


**Figure 2. Framework of Alignment and Disentanglement.** We begin by extracting roughly aligned features using a shared pre-trained backbone ( $\Phi$ ) through self-supervised contrastive learning. These features are then refined to be more independent and identifiable using two distinct linear mappings,  $H_S$  and  $H_E$ , optimized with Infomax loss (ICA). To support cross-domain alignment and prevent harmful permutations introduced by ICA, we apply identity initialization and orthogonal constraints. This framework effectively functions as a CCA method without paired annotations.

## 3. Method

In this section, we define the problem of synthetic image attribution and present our unsupervised framework, Alignment and Disentanglement (A&D), which identifies the source images behind synthetic outputs without the need for paired annotations. Our approach proceeds in two main stages: alignment, where contrastive self-supervised learning establishes an initial cross-domain similarity, and disentanglement, using Independent Component Analysis (ICA) to make learned features more independent and identifiable, thereby enhancing alignment. Furthermore, we provide a theoretical analysis of our A&D approach from a Canonical Correlation Analysis (CCA) perspective, specifying conditions that enable CCA to operate without paired data.

### 3.1. Problem: Synthetic Image Attribution

Synthetic image attribution focuses on identifying the source training image behind model-generated synthetics. In this paper, we focus on the challenging scenario described in (Wang et al., 2023), where only the training and synthetic images are accessible, without touching the model parameters. This setup is more realistic, as more generative models are becoming closed-source. Formally, consider two sets of images:  $X_S = \{\mathbf{x}_S^{(i)}\}_{i=1}^N \subset \mathcal{X}_S$ , which represents the synthetic images, and  $X_E = \{\mathbf{x}_E^{(j)}\}_{j=1}^M \subset \mathcal{X}_E$ , which represents the original training (exemplar) data. For convenience and aligning with (Wang et al., 2023), we use exemplar data/domain to represent the original training data in the following sections. In the supervised setting, the annotated dataset with synthesis-exemplar pairs

$\mathcal{D}_{paired} = \{(\mathbf{x}_S^{(k)}, \mathbf{x}_E^{(k)})\}_{k=1}^K$  are given. In our unsupervised setting, there is no paired data and only  $X_S$  and  $X_E$  are given.

The goal of synthetic image attribution is to learn two mapping functions,  $F_S : \mathbf{x}_S \rightarrow \mathbf{z}$  for the synthetic domain and  $F_E : \mathbf{x}_E \rightarrow \mathbf{z}$  for the exemplar domain, respectively. This allows us to match concepts and perform retrieval to identify the corresponding exemplar for a given synthetic image.

### 3.2. Alignment and Disentanglement

As the name suggests, our approach consists of two key stages: alignment through contrastive self-supervised learning and disentanglement using ICA. The overall framework is illustrated in Figure 2.

**Alignment.** The alignment is achieved by contrastive self-supervised learning, whose basic idea is optimizing embeddings so that positive pairs are closer and negative pairs are farther apart in a feature space. Formally, the objective function can be formulated as

$$\mathcal{L}_C^{i,j} = -\log \frac{\exp(\text{sim}(\mathbf{z}^{(i)}, \mathbf{z}^{(j)})/\tau)}{\sum_k \mathbb{I}_{[k \neq i]} \exp(\text{sim}(\mathbf{z}^{(i)}, \mathbf{z}^{(k)})/\tau)}, \quad (1)$$

where,  $\text{sim}(\cdot, \cdot)$  denotes the similarity metric, such as cosine similarity. Here,  $\mathbf{z}^{(i)}$  and  $\mathbf{z}^{(j)}$  denote the representations of the query and positive samples, respectively, which are typically generated by different augmentations. As the specifics of conducting contrastive learning are not the core contribution of this framework, we do not elaborate extensively here. We refer the reader to the references (He et al., 2020; Chen et al., 2020b; Caron et al., 2021) for more details.

Instead, we focus on explaining why self-supervised learning methods can achieve alignment. Leveraging the inherent data structure information, the alignment process highlights features that distinguish a sample from other “negative” samples. Despite the persistence of shifted domain information, this process establishes a basic feature space that facilitates rough matching between synthetics and exemplars. In our experiments, we observed that: 1) it is feasible to use pre-trained models without fine-tuning on the exemplars, and 2) with conservative training, the alignment progressively improves (shown in Table 2).

**Disentanglement.** After alignment, we apply ICA to further refine the representations of two domains, ensuring they conform to the same component-independent multivariate distribution. In particular, we introduce two distinct linear mappings,  $\mathbf{H}_S : \mathbf{z}_S \in \mathbb{R}^D \rightarrow \tilde{\mathbf{z}}_S \in \mathbb{R}^D$  and  $\mathbf{H}_E : \mathbf{z}_E \in \mathbb{R}^D \rightarrow \tilde{\mathbf{z}}_E \in \mathbb{R}^D$ , for the synthetic and exemplar domains, respectively.  $D$  is the dimension of the feature before and after ICA mapping. Each domain is fine-tuned using the objective function derived from the Infomax ICA principle (Bell & Sejnowski, 1995). For instance, in the synthetic

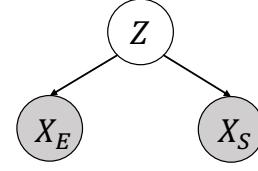


Figure 3. **Data generation process for CCA.** A shared latent variable  $Z$  generates two observation views,  $X_S$  and  $X_E$ , through different transformations.

domain, the Infomax loss function is expressed as:

$$\mathcal{L}_{IM}(X_S) = \ln |\mathbf{H}_S| + \mu \mathcal{L}_{Ent}, \quad (2)$$

where  $\mathbf{H}_S \in \mathbb{R}^{D \times D}$  denotes the weight matrix of the linear mapping.  $\mathcal{L}_{Ent}$  calculates the entropy of the latent variables:

$$\mathcal{L}_{Ent} = \frac{1}{ND} \sum_{i=1}^N \sum_{d=1}^D \ln \left( 1 - \tanh \left( \mathbf{h}_{S,d}^\top \mathbf{z}_S^{(i)} \right)^2 \right), \quad (3)$$

where  $\mathbf{h}_{S,d}$  is the  $d$ th column of the mapping matrix  $\mathbf{H}_S$  and  $\mathbf{z}_S^{(i)}$  denotes the feature of  $i$ th sample obtained by the alignment process. Then,  $\tilde{\mathbf{z}}_S^d = \mathbf{h}_{S,d}^\top \mathbf{z}_S^{(i)}$  produces the  $d$ th variable.  $\mu$  denotes the ratio of the entropy term.

Due to the permutation indeterminacy inherent in ICA (Car-doso & Souloumioc, 1993), the Infomax loss can identify independent components but cannot determine their order, resulting in output components that may be misaligned, which is detrimental to effective alignment. To solve this issue, we initialize the two mappings as identity matrices and impose orthogonality constraints on the weights:

$$\mathcal{L}_{Reg} = \|\mathbf{H}_S \mathbf{H}_S^\top - \mathbf{I}\|_F, \quad (4)$$

where  $\|A\|_F = \sqrt{\sum_{i,j} |a_{ij}|^2}$  represents the Frobenius norm.

Consequently, our loss function is expressed as:

$$\mathcal{L} = \mathcal{L}_{IM}(X_S) + \mathcal{L}_{IM}(X_E) + \lambda \mathcal{L}_{Reg}, \quad (5)$$

where  $\lambda$  is the hyper-parameter that balances the Infomax loss and the regularization term. In our approach, we treat the synthetic and exemplar domains equally, without involving another balancing coefficient. Visualization of features after disentanglement can be found in **Figure 12 in Appendix E**.

**Inference** During inference, given images from both domains, we process them through the entire A&D pipeline, encoding each image into its feature representation. We then calculate the cosine similarity between feature vectors across domains. The pairs with the highest cosine similarity are considered the most likely matches, providing the final attribution result.

### 3.3. Theoretical Analysis

Given our framework, one may ask why it works without paired data. In this section, we provide a theoretical analysis from a Canonical Correlation Analysis (CCA) perspective, explaining how and why our approach achieves CCA without paired data.

**CCA Framework.** The data generation process for CCA is illustrated in Figure 3, in which  $Z$  is a latent variable and  $\mathbf{X}_S, \mathbf{X}_E$  are two views generated from  $Z$  by different transformations. Then, the  $\mathbf{X}_S \in \mathbb{R}^{m_1}, \mathbf{X}_E \in \mathbb{R}^{m_2}$  denote random variables with covariances  $\Sigma_{11}, \Sigma_{22}$  and cross-covariance matrix  $\Sigma_{12}$ . CCA is concerned with finding a pair of linear transformations such that one component within each set of transformed variables is correlated with a single component in the other view (Bach & Jordan, 2005).

Then the target for CCA is to find  $(\mathbf{H}_S^\top \mathbf{X}_S, \mathbf{H}_E^\top \mathbf{X}_E)$  that are maximally correlated:

$$\begin{aligned} (\mathbf{H}_S^*, \mathbf{H}_E^*) &= \arg \max_{\mathbf{H}_S, \mathbf{H}_E} \text{corr}(\mathbf{H}_S^\top \mathbf{X}_S, \mathbf{H}_E^\top \mathbf{X}_E) \\ &= \arg \max_{\mathbf{H}_S, \mathbf{H}_E} \frac{\mathbf{H}_S^\top \Sigma_{12} \mathbf{H}_E}{\sqrt{\mathbf{H}_S^\top \Sigma_{11} \mathbf{H}_S \cdot \mathbf{H}_E^\top \Sigma_{22} \mathbf{H}_E}}. \end{aligned} \quad (6)$$

Equation 6 can be equivalently rewritten in the Lagrangian form as:

$$L = \underbrace{\mathbf{H}_S^\top \Sigma_{12} \mathbf{H}_E}_{\text{(a) cross-domain correlation}} - \underbrace{\frac{\lambda}{2} (\mathbf{H}_S^\top \Sigma_{11} \mathbf{H}_S - \mathbf{I}) - \frac{\lambda}{2} (\mathbf{H}_E^\top \Sigma_{22} \mathbf{H}_E - \mathbf{I})}_{\text{(b) within-domain uncorrelation}} \quad (7)$$

where  $\Sigma_{12} = \Phi(\mathbf{X}_S)\Phi(\mathbf{X}_E)^\top$ ,  $\Sigma_{11} = \Phi(\mathbf{X}_S)\Phi(\mathbf{X}_S)^\top$ ,  $\Sigma_{22} = \Phi(\mathbf{X}_E)\Phi(\mathbf{X}_E)^\top$ , and  $\mathbf{H}_S, \mathbf{H}_E \in \mathbb{R}^{d \times d}$  are linear mappings. Equation (7) decomposes CCA into two goals: (a) keep the two views maximally aligned through a large cross-domain correlation term  $\text{Tr}(\mathbf{H}_S^\top \Sigma_{12} \mathbf{H}_E)$ , and (b) enforce within-domain decorrelation/whitening. Our method mirrors this decomposition with a two-stage procedure that does not require paired samples.

**Stage I: find a shared feature space (alignment).** We first map both domains into a common representation space using a shared pretrained encoder  $\Phi$ , producing features  $\Phi(\mathbf{X}_S)$  and  $\Phi(\mathbf{X}_E)$  and the empirical cross-covariance  $\Sigma_{12} = \Phi(\mathbf{X}_S)\Phi(\mathbf{X}_E)^\top$ . Although we never observe paired  $(\mathbf{X}_S, \mathbf{X}_E)$ , we **hypothesize** that contrastive/self-supervised pretraining induces a common representation where the principal semantic axes are approximately aligned between the synthetic and exemplar domains. This is empirically supported by Table 1 where pretrained backbones alone already yields alignments to some extent. As a result,  $\Sigma_{12}$  already concentrates much of its mass on “matched” directions, yielding a rough CCA solution to (7).



Figure 4. Examples of Exemplar (top) and Synthetic (bottom) images in the AbC benchmark.

**Stage II: within-domain uncorrelation while preserving cross-domain alignment. (disentanglement)** We refine each domain with ICA (Infomax) to promote independence, which is a stricter requirement than the uncorrelation constraints in CCA. With the constraint Equation (4), we enforce  $\mathbf{H}_E \mathbf{H}_S^\top = \mathbf{I}$ . Using the cyclic property of the trace operator, we have:  $\text{Tr}(\mathbf{H}_S^\top \Sigma_{12} \mathbf{H}_E) = \text{Tr}(\Sigma_{12} \mathbf{H}_E \mathbf{H}_S^\top) = \text{Tr}(\Sigma_{12})$  which means that we can optimize the objective in Equation (7)(b) while keeping Equation (7)(a) unchanged, yielding an improved CCA solution. Intuitively, ICA is used to “clean up” each view internally (better separated components), while the identity-biased orthogonal updates prevent the well-aligned cross-domain directions encoded in  $\Sigma_{12}$  from being destroyed by ICA’s permutation/rotation ambiguity. Empirically, we found that replacing Equation (4) with  $\frac{1}{2} (\|\mathbf{H}_E \mathbf{H}_E^\top - \mathbf{I}\|_F + \|\mathbf{H}_S \mathbf{H}_S^\top - \mathbf{I}\|_F)$  yields better results, thus we conduct experiments with this constraint. Equation (4) is also effective; results are in Appendix F.

## 4. Experiments

### 4.1. Datasets and Evaluation Metrics

In the experiments, we apply the AbC (Attribution by Customization) benchmark (Wang et al., 2023), which is specifically designed to evaluate synthetic image attribution for generative models, utilizing Custom Diffusion (Kumari et al., 2023) to generate over 4 million synthesized images influenced by particular exemplar images or artistic styles. It encompasses both object-centric and artistic style synthesis-exemplar image pairs, created using a variety of prompts. Some examples are shown in Figure 4, and more can be found in Appendix E. The benchmark serves as a valuable resource for testing and enhancing attribution algorithms.

The training set consists of three distinct categories: object-centric, artistic styles, and a combination of object-centric and artistic styles. The object-centric images include various object categories sourced from ImageNet (Geirhos et al., 2018), while the artistic style images are drawn from the BAM-FG (Behance Artistic Media - FineGrained) dataset (Ruta et al., 2021). The test set is divided into four splits: ImageNet-Seen, BAM-FG, ImageNet-Unseen, and Artchive (Harden). The ImageNet-Seen split contains object cate-



**Figure 5. Attribution results visualization.** We start with a synthetic image generated by CustomDiffusion (based on Stable Diffusion) and retrieve its exemplars from a pool of 1 million LAION images, showing the top 10 results. *Alignment* denotes attribution using the pretrained DINO model, *Supervised* refers to DINO fine-tuned with paired training data from the AbC benchmark, and A&D is our proposed unsupervised fine-tuning method. Red bounding boxes indicate the ground-truth exemplars.

gories that are present in the training set, and the BAM-FG split includes artistic styles that are the same as the training data. These two splits serve as in-distribution test cases, closely reflecting the training set’s content. In contrast, the ImageNet-Unseen split comprises object categories absent from the training set, and the Artchive split features artistic styles distinct from those encountered during training. These splits are designed to evaluate the model’s generalization to out-of-distribution data. Additionally, “GPT,” “Media,” and “Object” denote different methods of prompting used to generate the synthetic images.

Our evaluation setting follows the approach in (Wang et al., 2023). For each synthetic image in the test set, we retrieve its exemplar images from a dataset comprising the exemplars and 1 million images from the LAION dataset (Schuhmann et al., 2022). The metrics used include Recall@K, which measures the proportion of exemplar images among the top-K retrieved results, and mAP, which evaluates the overall ordering of the retrieval results. Further details about these metrics can be found in the Appendix C.

#### 4.2. Implementation details

For alignment, we experimented with different pretrained models, including contrastive self-supervised approaches (MoCo V3 (Chen et al., 2021) and DINO (Caron et al., 2021)), a supervised method (ViT (Dosovitskiy et al., 2020)), and a copy detection model (SSCD (Pizzi et al., 2022)). To ensure fair comparison, we used the same ViT-B/16 backbone architecture across MoCo, DINO, and ViT. For disentanglement, we fine-tuned two separate square linear mappings for the two domains using the Adam optimizer (Kingma & Ba, 2014), with a learning rate of 0.001. We set two hyperparameters:  $\lambda$  controls  $\mathcal{L}_{Reg}$  and  $\mu$  controls  $\mathcal{L}_{IM}$ . The values of  $\lambda$  were set to 0.1 for MoCo, DINO, and CLIP, and 0.15 for ViT and SSCD, while  $\mu$  was set to 1e3 for MoCo and 1 for all others. Our models were fine-tuned on a single A100 40G GPU with a batch size of 512 for ViT and 1024 for the other models. All the experiments are implemented by Pytorch 2.3.0.

#### 4.3. Comparison with other methods

We conducted a comprehensive evaluation of our proposed A&D method against several other approaches, including both supervised and unsupervised methods: Supervised Learning (Wang et al., 2023), Pseudo Labeling (Lee et al., 2013), and Pretraining (inference without further finetuning). The models were tuned on three training sets from the AbC benchmark: (1) object-centric, (2) artistic styles, and (3) a combination of both. We evaluated the performance of models trained on the combined training set (3) across all test sets, with results presented in terms of Recall@5 and mAP, as shown in Table 1.

Our method, A&D, a fully unsupervised approach, outperformed all other methods, including supervised ones, in the average of both Recall@5 and mAP across MoCo, DINO, and ViT backbones. Notably, A&D achieved the highest average Recall@5 (0.386) and mAP (0.370) with the DINO backbone. Compared to other unsupervised methods, our approach outperformed all except Pseudo Labeling on the SSCD backbone, where it was only 0.3% and 0.1% lower in Recall@5 and mAP, respectively. On the ImageNet-Unseen Media test set, our A&D method, using MoCo as the alignment backbone, outperformed Pretraining, Pseudo Labeling, and Supervised methods by 10.9%, 11.7%, and 5% in Recall@5, and by 10.4%, 11%, and 4.5% in mAP, respectively. These results underscore the effectiveness of our unsupervised method for synthetic image attribution. Additional experimental results on the AbC benchmark can be found in Appendix G, and visualization of attribution results can be found in Appendix D.

We also visualize the retrieved results in Figure 5. Compared with using the alignment backbone alone (Alignment) or supervised fine-tuning (Supervised), our A&D tends to produce more fine-grained concept matching. In the example shown, Alignment and Supervised mainly retrieve images that share the coarse concept (“mosque”) but vary substantially in viewpoint and architectural details, whereas A&D ranks exemplars that better preserve the specific visual cues of the query—e.g., a similar frontal composition

**Table 1. R@5 and mAP of four scenarios on AbC benchmark.** We compare A&D with both supervised method and unsupervised methods (Pretrain, Pseudo label (Lee et al., 2013)) on five different backbones across four subdatasets. We empirically find that A&D outperforms the unsupervised baselines in all settings except for Pseudo Labeling using the SSCD backbone and, surprisingly, surpasses the supervised method when using the MOCO, DINO, and ViT as backbones.

Source	ImageNet-Seen				BAM-FG				ImageNet-Unseen				Artchive				Average	
	Prompts		GPT	Media	GPT		Object	GPT		Media	GPT		Object	GPT		Object		
$F_{\text{base}}$	Method	R@5	mAP	R@5	mAP	R@5	mAP	R@5	mAP	R@5	mAP	R@5	mAP	R@5	mAP	R@5	mAP	
Pretrain	0.390	0.347	0.239	0.211	0.130	0.144	0.187	0.211	0.761	0.717	0.460	0.408	0.169	0.164	0.131	0.125	0.308	0.291
	Pseudo	0.418	0.377	0.251	0.221	0.132	0.146	0.187	0.212	0.778	0.736	0.452	0.402	0.166	0.162	0.132	0.128	0.315
MoCo A&D	0.444	0.399	0.313	0.277	0.157	0.175	0.209	0.238	0.804	0.765	0.569	0.512	0.204	0.204	0.158	0.154	<b>0.357</b>	<b>0.341</b>
	Superv	0.437	0.394	0.295	0.262	0.153	0.172	0.209	0.238	0.791	0.753	0.519	0.467	0.208	0.209	0.165	0.165	0.347
Pretrain	0.433	0.393	0.288	0.255	0.148	0.163	0.193	0.219	0.831	0.795	0.540	0.492	0.183	0.181	0.140	0.136	0.345	0.329
	Pseudo	0.471	0.426	0.374	0.330	0.127	0.142	0.164	0.187	0.840	0.804	0.639	0.588	0.211	0.216	0.161	0.160	0.373
DINO A&D	0.491	0.448	0.364	0.323	0.167	0.186	0.210	0.239	0.845	0.811	0.633	0.581	0.212	0.214	0.164	0.161	<b>0.386</b>	<b>0.370</b>
	Superv	0.475	0.433	0.351	0.311	0.165	0.184	0.212	0.239	0.842	0.810	0.598	0.549	0.217	0.221	0.170	0.169	0.379
Pretrain	0.355	0.310	0.242	0.210	0.168	0.193	0.224	0.259	0.785	0.726	0.474	0.410	0.201	0.210	0.156	0.161	0.326	0.310
	Pseudo	0.361	0.319	0.266	0.230	0.103	0.117	0.141	0.162	0.794	0.737	0.525	0.457	0.156	0.161	0.115	0.114	0.308
ViT A&D	0.440	0.395	0.295	0.259	0.203	0.229	0.251	0.288	0.845	0.805	0.561	0.500	0.229	0.240	0.176	0.182	<b>0.375</b>	<b>0.362</b>
	Superv	0.475	0.433	0.351	0.311	0.165	0.184	0.212	0.239	0.842	0.810	0.598	0.549	0.217	0.221	0.170	0.169	0.379
Pretrain	0.236	0.195	0.137	0.118	0.129	0.148	0.174	0.200	0.580	0.500	0.239	0.201	0.186	0.198	0.140	0.144	0.228	0.213
	Pseudo	0.018	0.015	0.014	0.011	0.022	0.026	0.032	0.036	0.032	0.027	0.009	0.007	0.185	0.212	0.147	0.161	0.057
CLIP A&D	0.257	0.212	0.153	0.132	0.173	0.202	0.216	0.251	0.607	0.525	0.258	0.218	0.229	0.256	0.176	0.190	0.259	0.248
	Superv	0.329	0.280	0.222	0.190	0.186	0.219	0.236	0.278	0.701	0.633	0.389	0.332	0.259	0.297	0.201	0.223	<b>0.315</b>
Pretrain	0.253	0.230	0.142	0.131	0.117	0.128	0.175	0.194	0.601	0.566	0.264	0.245	0.151	0.142	0.123	0.115	0.228	0.219
	Pseudo	0.267	0.241	0.154	0.140	0.110	0.118	0.161	0.178	0.618	0.581	0.285	0.263	0.156	0.147	0.126	0.119	0.235
SSCD A&D	0.259	0.234	0.147	0.134	0.119	0.130	0.176	0.196	0.610	0.573	0.272	0.251	0.150	0.142	0.123	0.115	0.232	0.222
	Superv	0.268	0.242	0.156	0.142	0.118	0.128	0.314	0.193	0.621	0.586	0.282	0.261	0.159	0.150	0.131	0.123	<b>0.256</b>

with the two tall minarets framing the central dome and sharper, peaked silhouettes—thereby yielding a more detailed cross-domain alignment. More examples can be found in [Appendix Figure 10](#).

#### 4.4. Discussion

**What’s the Difference between Our A&D and Adaptation?** We would like to highlight that our approach is not simply an adaptation of pretrained models under distribution shift, where fine-tuning on new data could be sufficient—a direction that has been widely explored in prior work. While adaptation typically involves a single domain undergoing distribution shift, our A&D framework considers two distinct domains, making it conceptually different. In contrast, our A&D framework operates across two distinct domains. To empirically validate this distinction, we fine-tuned DINO on the BAM-FG exemplar training set for 10 epochs and used the resulting model as the alignment backbone in our disentanglement process. As shown in Table 2, fine-tuning DINO on BAM-FG yields only marginal improvements, with less than a 1% increase in both Recall@5 and mAP on the BAM-FG test set. Furthermore, comparing the two DINO models as alignment backbones

**Table 2. Performance of DINO tuned on BAM-FG.** “Pretrain” refers to the original DINO model, “Tuned” indicates the DINO model further fine-tuned for 10 epochs on BAM-FG, and “Tuned+A&D” denotes the model trained on the object + style training set of Abc.

Source	BAM-FG		
	Prompts	GPT	Object
$F_{\text{base}}$	Method	R@5	mAP
DINO	Pretrain	0.148	0.163
	Tuned	0.154	0.172
	A&D	<b>0.167</b>	<b>0.186</b>
	Tuned+A&D	0.162	0.184

reveals that fine-tuning on exemplars does not meaningfully enhance A&D performance, as Recall@5 and mAP remain nearly unchanged with or without fine-tuning.

**Why Supervised Methods Underperform Unsupervised?** The supervised method underperforms due to the ambiguous nature of the supervision. Such noise may introduce misleading signals, resulting in suboptimal performance. An example of the dataset is shown in Figure 11.

**Why the Moderate Performance?** The moderate performance of A&D with CLIP and SSCD can be attributed to the

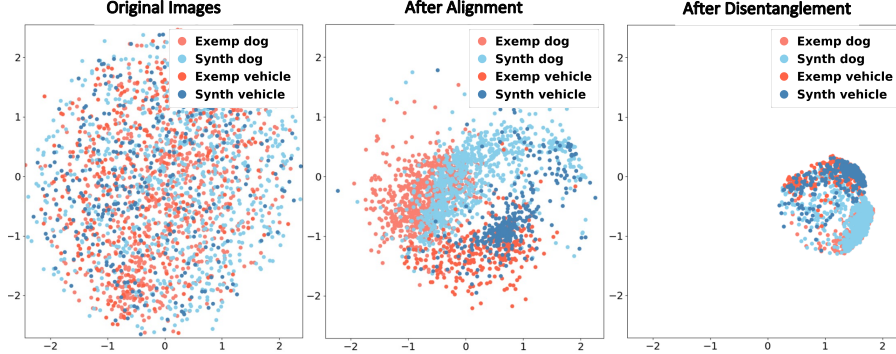


**Figure 6. Scatter Plot of Distribution Changes through A&D using MoCo alignment backbone.** The scatter plot illustrates the feature distribution changes for two categories of images from AbC’s object-centric training set: dog and vehicle. The original data points appear almost random, with little to no alignment between domains. After alignment, we observe that corresponding objects from the two views become more closely matched. With disentanglement, this alignment becomes significantly more distinct and precise, demonstrating the effectiveness of our A&D framework.

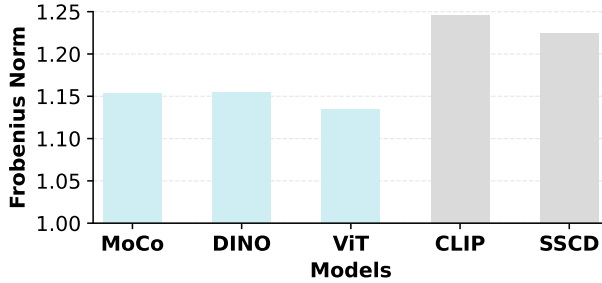


**Figure 7. F-norms for Different Backbone Models.** We show the F-norm of the difference between the covariance matrix of synthetic and exemplar features from AbC’s object-centric training set and identity matrix, compared across different pretrained backbone models. The lower F-norms observed for MoCo, DINO, and ViT compared to CLIP and SSCD indicate better alignment.

inherent characteristics of these models. CLIP, trained using two different modalities—text and image—might not produce representations that are well-suited for cross-domain image alignment. The pseudo-labeling results for CLIP in Table 1 reveal that using pretrained CLIP actually misdirects the training process, leading to suboptimal alignment. This observation is further supported by the Frobenius norm analysis in Figure 7. For SSCD, which is a contrastive self-supervised backbone specifically trained for copy detection, our A&D framework underperforms compared to even pseudo-labeling. We believe this is because SSCD’s learned features are specialized for copy detection, lacking the generalization needed to effectively represent more complex image distributions across domains.

**Distribution Visualization** Figure 6 demonstrates the efficacy of our proposed framework in aligning features across domains. We selected two object categories (vehicle and dog) from AbC’s object-centric training set and visualized their feature distribution changes. In these scatter plots, red points correspond to images from the exemplar domain,

while blue points represent images from the synthetic domain. Point darkness encodes category shared across domains: darker points denote one category, lighter points the other. Initially, the distributions of the original images are scattered randomly, showing significant overlap and poor cross-domain alignment. After passing the alignment backbone which we used MoCo here, while not perfect, there is a noticeable grouping of the same category across domains, indicating that we have successfully started to align the features. After disentanglement, the distributions tighten and separate more clearly by category, indicating improved cross-domain alignment. This refinement highlights disentanglement’s role in achieving stronger alignment.

## 5. Conclusion

In this paper, we have proposed an unsupervised framework for synthetic image attribution, termed Alignment and Disentanglement. Our approach eliminates the need for paired annotations by using contrastive self-supervised learning for alignment and ICA for disentanglement. Through theoretical analysis, we demonstrated that our framework aligns with the CCA framework under some intuitive assumptions, offering a new perspective on implementing CCA without paired data. Our extensive experiments on the AbC benchmark show that A&D not only matches but, in some cases, surpasses the performance of the supervised method. **Limitations:** we assume access to a pretrained backbone with reasonable cross-domain alignment; addressing larger domain gaps is an important direction for future work. One solution is to add an explicit cross-domain alignment stage, trained with self-supervision and stability regularization, to better handle large domain gaps. We hope that this work, including the findings and algorithm, will shed light on more efficient approaches for synthetic image attribution and inspire further research to design more effective methods.

## Impact Statement

This paper presents work whose goal is to advance the field of Machine Learning. There are many potential societal consequences of our work, none which we feel must be specifically highlighted here.

## References

Andrew, G., Arora, R., Bilmes, J., and Livescu, K. Deep canonical correlation analysis. In *International conference on machine learning*, pp. 1247–1255. PMLR, 2013.

Bach, F. R. and Jordan, M. I. Kernel independent component analysis. *Journal of machine learning research*, 3(Jul):1–48, 2002.

Bach, F. R. and Jordan, M. I. A probabilistic interpretation of canonical correlation analysis. 2005.

Bell, A. J. and Sejnowski, T. J. An information-maximization approach to blind separation and blind deconvolution. *Neural computation*, 7(6):1129–1159, 1995.

Bui, T., Yu, N., and Collomosse, J. Repmix: Representation mixing for robust attribution of synthesized images. In *European Conference on Computer Vision*, pp. 146–163. Springer, 2022.

Burgess, C. P., Higgins, I., Pal, A., Matthey, L., Watters, N., Desjardins, G., and Lerchner, A. Understanding disentangling in  $\beta$ -vae. *arXiv preprint arXiv:1804.03599*, 2018.

Cardoso, J.-F. and Souloumiac, A. Blind beamforming for non-gaussian signals. In *IEE proceedings F (radar and signal processing)*, volume 140, pp. 362–370. IET, 1993.

Carlini, N., Tramer, F., Wallace, E., Jagielski, M., Herbert-Voss, A., Lee, K., Roberts, A., Brown, T., Song, D., Erlingsson, U., et al. Extracting training data from large language models. In *30th USENIX Security Symposium (USENIX Security 21)*, pp. 2633–2650, 2021.

Caron, M., Touvron, H., Misra, I., Jégou, H., Mairal, J., Bojanowski, P., and Joulin, A. Emerging properties in self-supervised vision transformers. In *Proceedings of the IEEE/CVF international conference on computer vision*, pp. 9650–9660, 2021.

Chen, D., Yu, N., Zhang, Y., and Fritz, M. Gan-leaks: A taxonomy of membership inference attacks against generative models. In *Proceedings of the 2020 ACM SIGSAC conference on computer and communications security*, pp. 343–362, 2020a.

Chen, R. T., Li, X., Grosse, R. B., and Duvenaud, D. K. Isolating sources of disentanglement in variational autoencoders. *Advances in neural information processing systems*, 31, 2018.

Chen, T., Kornblith, S., Norouzi, M., and Hinton, G. A simple framework for contrastive learning of visual representations. In *International conference on machine learning*, pp. 1597–1607. PMLR, 2020b.

Chen, X., Xie, S., and He, K. An empirical study of training self-supervised vision transformers. In *Proceedings of the IEEE/CVF international conference on computer vision*, pp. 9640–9649, 2021.

Comon, P. Independent component analysis, a new concept? *Signal processing*, 36(3):287–314, 1994.

Dai, Z. and Gifford, D. K. Training data attribution for diffusion models. *arXiv preprint arXiv:2306.02174*, 2023.

Denton, E. L. et al. Unsupervised learning of disentangled representations from video. *Advances in neural information processing systems*, 30, 2017.

Dosovitskiy, A., Beyer, L., Kolesnikov, A., Weissenborn, D., Zhai, X., Unterthiner, T., Dehghani, M., Minderer, M., Heigold, G., Gelly, S., et al. An image is worth 16x16 words: Transformers for image recognition at scale. *arXiv preprint arXiv:2010.11929*, 2020.

Feldman, V. and Zhang, C. What neural networks memorize and why: Discovering the long tail via influence estimation. *Advances in Neural Information Processing Systems*, 33:2881–2891, 2020.

Geirhos, R., Rubisch, P., Michaelis, C., Bethge, M., Wichmann, F. A., and Brendel, W. Imagenet-trained cnns are biased towards texture; increasing shape bias improves accuracy and robustness. *arXiv preprint arXiv:1811.12231*, 2018.

Georgiev, K., Vendrow, J., Salman, H., Park, S. M., and Madry, A. The journey, not the destination: How data guides diffusion models. *arXiv preprint arXiv:2312.06205*, 2023.

Ghorbani, A. and Zou, J. Data shapley: Equitable valuation of data for machine learning. In *International conference on machine learning*, pp. 2242–2251. PMLR, 2019.

Hälvä, H. and Hyvärinen, A. Hidden markov nonlinear ica: Unsupervised learning from nonstationary time series. In *Conference on Uncertainty in Artificial Intelligence*, pp. 939–948. PMLR, 2020.

Harden, M. Mark harden’s archive. URL <https://www.artchive.com/>.

Hayes, J., Melis, L., Danezis, G., and De Cristofaro, E. Logan: Membership inference attacks against generative models. *arXiv preprint arXiv:1705.07663*, 2017.

He, K., Fan, H., Wu, Y., Xie, S., and Girshick, R. Momentum contrast for unsupervised visual representation learning. In *Proceedings of the IEEE/CVF conference on computer vision and pattern recognition*, pp. 9729–9738, 2020.

Higgins, I., Amos, D., Pfau, D., Racaniere, S., Matthey, L., Rezende, D., and Lerchner, A. Towards a definition of disentangled representations. *arXiv preprint arXiv:1812.02230*, 2018.

Hilprecht, B., Härtelrich, M., and Bernau, D. Monte carlo and reconstruction membership inference attacks against generative models. *Proceedings on Privacy Enhancing Technologies*, 2019.

Hotelling, H. Relations between two sets of variates. In *Breakthroughs in statistics: methodology and distribution*, pp. 162–190. Springer, 1992.

Hu, H., Salcic, Z., Sun, L., Dobbie, G., Yu, P. S., and Zhang, X. Membership inference attacks on machine learning: A survey. *ACM Computing Surveys (CSUR)*, 54(11s):1–37, 2022.

Huber, P. J. and Ronchetti, E. M. *Robust statistics*. John Wiley & Sons, 2011.

Hyvärinen, A., Karhunen, J., and Oja, E. Independent component analysis and blind source separation, 2001.

Hyvärinen, A., Sasaki, H., and Turner, R. Nonlinear ica using auxiliary variables and generalized contrastive learning. In *The 22nd International Conference on Artificial Intelligence and Statistics*, pp. 859–868. PMLR, 2019.

Jia, R., Dao, D., Wang, B., Hubis, F. A., Gurel, N. M., Li, B., Zhang, C., Spanos, C. J., and Song, D. Efficient task-specific data valuation for nearest neighbor algorithms. *arXiv preprint arXiv:1908.08619*, 2019.

Jia, R., Wu, F., Sun, X., Xu, J., Dao, D., Kailkhura, B., Zhang, C., Li, B., and Song, D. Scalability vs. utility: Do we have to sacrifice one for the other in data importance quantification? In *Proceedings of the IEEE/CVF Conference on Computer Vision and Pattern Recognition*, pp. 8239–8247, 2021.

Kandpal, N., Wallace, E., and Raffel, C. Deduplicating training data mitigates privacy risks in language models. In *International Conference on Machine Learning*, pp. 10697–10707. PMLR, 2022.

Kingma, D. P. Auto-encoding variational bayes. *arXiv preprint arXiv:1312.6114*, 2013.

Kingma, D. P. and Ba, J. Adam: A method for stochastic optimization. *arXiv preprint arXiv:1412.6980*, 2014.

Koh, P. W. and Liang, P. Understanding black-box predictions via influence functions. In *International conference on machine learning*, pp. 1885–1894. PMLR, 2017.

Koh, P. W. W., Ang, K.-S., Teo, H., and Liang, P. S. On the accuracy of influence functions for measuring group effects. *Advances in neural information processing systems*, 32, 2019.

Kumari, N., Zhang, B., Zhang, R., Shechtman, E., and Zhu, J.-Y. Multi-concept customization of text-to-image diffusion. In *Proceedings of the IEEE/CVF Conference on Computer Vision and Pattern Recognition*, pp. 1931–1941, 2023.

Kwon, Y. and Zou, J. Beta shapley: a unified and noise-reduced data valuation framework for machine learning. *arXiv preprint arXiv:2110.14049*, 2021.

Lachapelle, S., Rodriguez, P., Sharma, Y., Everett, K. E., Le Priol, R., Lacoste, A., and Lacoste-Julien, S. Disentanglement via mechanism sparsity regularization: A new principle for nonlinear ica. In *Conference on Causal Learning and Reasoning*, pp. 428–484. PMLR, 2022.

Law, J. Robust statistics—the approach based on influence functions, 1986.

Lee, D.-H. et al. Pseudo-label: The simple and efficient semi-supervised learning method for deep neural networks. In *Workshop on challenges in representation learning, ICML*, volume 3, pp. 896. Atlanta, 2013.

Lee, H.-Y., Tseng, H.-Y., Huang, J.-B., Singh, M., and Yang, M.-H. Diverse image-to-image translation via disentangled representations. In *Proceedings of the European conference on computer vision (ECCV)*, pp. 35–51, 2018.

Lin, J., Tao, L., Dong, M., and Xu, C. Diffusion attribution score: Evaluating training data influence in diffusion models. *arXiv preprint arXiv:2410.18639*, 2024.

Lindenbaum, O., Yeredor, A., Salhov, M., and Averbuch, A. Multi-view diffusion maps. *Information Fusion*, 55: 127–149, 2020.

Lu, A., Wang, W., Bansal, M., Gimpel, K., and Livescu, K. Deep multilingual correlation for improved word embeddings. In *Proceedings of the 2015 conference of the North American chapter of the association for computational linguistics: human language technologies*, pp. 250–256, 2015.

Lu, D., Wang, S.-Y., Kumari, N., Agarwal, R., Tang, M., Bau, D., and Zhu, J.-Y. Content-based search for deep

generative models. In *SIGGRAPH Asia 2023 Conference Papers*, pp. 1–12, 2023.

Marra, F., Gragnaniello, D., Verdoliva, L., and Poggi, G. Do gans leave artificial fingerprints? In *2019 IEEE conference on multimedia information processing and retrieval (MIPR)*, pp. 506–511. IEEE, 2019.

Michaeli, T., Wang, W., and Livescu, K. Nonparametric canonical correlation analysis. In *International conference on machine learning*, pp. 1967–1976. PMLR, 2016.

Misra, I. and Maaten, L. v. d. Self-supervised learning of pretext-invariant representations. In *Proceedings of the IEEE/CVF conference on computer vision and pattern recognition*, pp. 6707–6717, 2020.

Mlodzeniec, B., Eschenhagen, R., Bae, J., Immer, A., Krueger, D., and Turner, R. Influence functions for scalable data attribution in diffusion models. *arXiv preprint arXiv:2410.13850*, 2024.

Park, S. M., Georgiev, K., Ilyas, A., Leclerc, G., and Madry, A. Trak: Attributing model behavior at scale. *arXiv preprint arXiv:2303.14186*, 2023.

Pizzi, E., Roy, S. D., Ravindra, S. N., Goyal, P., and Douze, M. A self-supervised descriptor for image copy detection. In *Proceedings of the IEEE/CVF Conference on Computer Vision and Pattern Recognition*, pp. 14532–14542, 2022.

Radford, A., Kim, J. W., Hallacy, C., Ramesh, A., Goh, G., Agarwal, S., Sastry, G., Askell, A., Mishkin, P., Clark, J., et al. Learning transferable visual models from natural language supervision. In *International conference on machine learning*, pp. 8748–8763. PMLR, 2021.

Ramesh, A., Dhariwal, P., Nichol, A., Chu, C., and Chen, M. Hierarchical text-conditional image generation with clip latents. *arXiv preprint arXiv:2204.06125*, 1(2):3, 2022.

Rombach, R., Blattmann, A., Lorenz, D., Esser, P., and Ommer, B. High-resolution image synthesis with latent diffusion models. In *Proceedings of the IEEE/CVF conference on computer vision and pattern recognition*, pp. 10684–10695, 2022.

Ruta, D., Motiian, S., Faieta, B., Lin, Z., Jin, H., Filipkowski, A., Gilbert, A., and Collomosse, J. Aladin: All layer adaptive instance normalization for fine-grained style similarity. In *Proceedings of the IEEE/CVF International Conference on Computer Vision*, pp. 11926–11935, 2021.

Sablayrolles, A., Douze, M., Schmid, C., and Jégou, H. D\’ej\`a vu: an empirical evaluation of the memorization properties of convnets. *arXiv preprint arXiv:1809.06396*, 2018.

Saharia, C., Chan, W., Saxena, S., Li, L., Whang, J., Denton, E. L., Ghasemipour, K., Gontijo Lopes, R., Karagol Ayan, B., Salimans, T., et al. Photorealistic text-to-image diffusion models with deep language understanding. *Advances in neural information processing systems*, 35: 36479–36494, 2022.

Schioppa, A., Zablotskaia, P., Vilar, D., and Sokolov, A. Scaling up influence functions. In *Proceedings of the AAAI Conference on Artificial Intelligence*, volume 36, pp. 8179–8186, 2022.

Schuhmann, C., Beaumont, R., Vencu, R., Gordon, C., Wightman, R., Cherti, M., Coombes, T., Katta, A., Mullis, C., Wortsman, M., et al. Laion-5b: An open large-scale dataset for training next generation image-text models. *Advances in Neural Information Processing Systems*, 35: 25278–25294, 2022.

Sha, Z., Li, Z., Yu, N., and Zhang, Y. De-fake: Detection and attribution of fake images generated by text-to-image generation models. In *Proceedings of the 2023 ACM SIGSAC Conference on Computer and Communications Security*, pp. 3418–3432, 2023.

Sharchilev, B., Ustinovskiy, Y., Serdyukov, P., and Rijke, M. Finding influential training samples for gradient boosted decision trees. In *International Conference on Machine Learning*, pp. 4577–4585. PMLR, 2018.

Shokri, R., Stronati, M., Song, C., and Shmatikov, V. Membership inference attacks against machine learning models. In *2017 IEEE symposium on security and privacy (SP)*, pp. 3–18. IEEE, 2017.

Sorrenson, P., Rother, C., and Köthe, U. Disentanglement by nonlinear ica with general incompressible-flow networks (gin). *arXiv preprint arXiv:2001.04872*, 2020.

Tian, Y., Krishnan, D., and Isola, P. Contrastive multiview coding. In *Computer Vision–ECCV 2020: 16th European Conference, Glasgow, UK, August 23–28, 2020, Proceedings, Part XI 16*, pp. 776–794. Springer, 2020.

Wang, S.-Y., Efros, A. A., Zhu, J.-Y., and Zhang, R. Evaluating data attribution for text-to-image models. In *Proceedings of the IEEE/CVF International Conference on Computer Vision*, pp. 7192–7203, 2023.

Wang, S.-Y., Hertzmann, A., Efros, A. A., Zhu, J.-Y., and Zhang, R. Data attribution for text-to-image models by unlearning synthesized images. *arXiv preprint arXiv:2406.09408*, 2024.

Wang, S.-Y., Hertzmann, A., Efros, A. A., Zhang, R., and Zhu, J.-Y. Fast data attribution for text-to-image models. *arXiv preprint arXiv:2511.10721*, 2025.

Wang, W., Arora, R., Livescu, K., and Bilmes, J. A. Unsupervised learning of acoustic features via deep canonical correlation analysis. In *2015 IEEE International Conference on Acoustics, Speech and Signal Processing (ICASSP)*, pp. 4590–4594. IEEE, 2015.

Yu, N., Davis, L. S., and Fritz, M. Attributing fake images to gans: Learning and analyzing gan fingerprints. In *Proceedings of the IEEE/CVF international conference on computer vision*, pp. 7556–7566, 2019.

Zhao, Y., Du, C., Zheng, X., Pang, T., and Lin, M. Non-parametric data attribution for diffusion models. *arXiv preprint arXiv:2510.14269*, 2025.

Zheng, X., Pang, T., Du, C., Jiang, J., and Lin, M. Intriguing properties of data attribution on diffusion models. *arXiv preprint arXiv:2311.00500*, 2023.

Zheng, Z. and Sun, L. Disentangling latent space for vae by label relevant/irrelevant dimensions. In *Proceedings of the IEEE/CVF Conference on Computer Vision and Pattern Recognition*, pp. 12192–12201, 2019.

# Appendix

## A. Difference from Model Attribution

For a synthesized image, recent works have focused on identifying the image’s source model (Yu et al., 2019; Bui et al., 2022; Marra et al., 2019; Sha et al., 2023) or determining which model can best represent it (Lu et al., 2023), a field known as model attribution. In the context of GAN-based models, membership inference, an open problem, has been explored for both generative (Hayes et al., 2017; Hilprecht et al., 2019; Chen et al., 2020a; Carlini et al., 2021) and discriminative (Shokri et al., 2017; Sablayrolles et al., 2018; Hu et al., 2022) models. The main difference in our work is that we don’t focus on the model, but rather on the synthesized images and their corresponding training data.

## B. Setting Comparison with Domain Generalization

While our approach and domain generalization share the high-level goal of bridging two domains, the underlying assumptions about the data generation process are fundamentally different, below we show the detailed difference of the data generation process. An illustration of the difference is given in Figure 8.

**Domain generalization.** A common assumption in domain generalization is that data from different domains are generated from a shared invariant latent variable  $\mathbf{Z}^c$  and domain-specific variables  $\mathbf{Z}_E^s$  and  $\mathbf{Z}_S^s$ . Specifically, the generation follows:

$$\mathbf{X}_E = g(\mathbf{Z}^c, \mathbf{Z}_E^s) \quad \text{and} \quad \mathbf{X}_S = g(\mathbf{Z}^c, \mathbf{Z}_S^s), \quad (8)$$

where the generation function  $g$  is shared. The objective is to recover  $\mathbf{Z}^c$ —the shared, invariant component—across multiple domains, enabling better generalization to unseen ones.

**Our framework.** In contrast, our framework assumes that both  $\mathbf{X}_E$  and  $\mathbf{X}_S$  are generated from a single shared latent variable  $\mathbf{Z}$ , but through distinct functions:

$$\mathbf{X}_E = g_E(\mathbf{Z}, \epsilon_E) \quad \text{and} \quad \mathbf{X}_S = g_S(\mathbf{Z}, \epsilon_S), \quad (9)$$

where  $\epsilon_E$  and  $\epsilon_S$  are independent noise terms. Instead of recovering a shared component from partially shared inputs, we aim to learn two distinct functions that map both  $\mathbf{X}_E$  and  $\mathbf{X}_S$  into a common latent space  $\mathbf{Z}$ .

## C. Evaluation Metric Details

**Recall@k** measures the fraction of relevant exemplar images that are successfully retrieved among the top-k results. It is computed as:

$$\text{Recall}@k = \frac{n_e}{n_a},$$

where  $n_e$  is the number of  $X_e^{(i)}$  in top k,  $n_a$  is total number of  $X_e^{(i)}$ .

**Mean Average Precision(mAP)** takes into account both the precision and ranking quality of the retrieved results. The Average Precision (AP) for a single synthetic image is calculated as:

$$\text{AP} = \sum_{k=1}^m \left( \frac{P(k) \cdot \text{Rel}(k)}{n_e} \right),$$

where  $P(k)$  is the precision at cut-off  $k$  in the list,  $\text{Rel}(k)$  is an indicator function equaling 1 if the item at rank  $k$  is a matched exemplar image, and 0 otherwise.  $m$  is the total number of images retrieved.

The mAP is then computed as the mean of AP scores over all synthetic images used for evaluation:

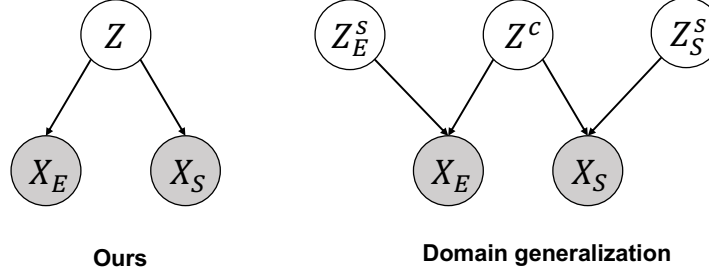


Figure 8. Data generation process for comparing the difference between our framework and domain generalization.

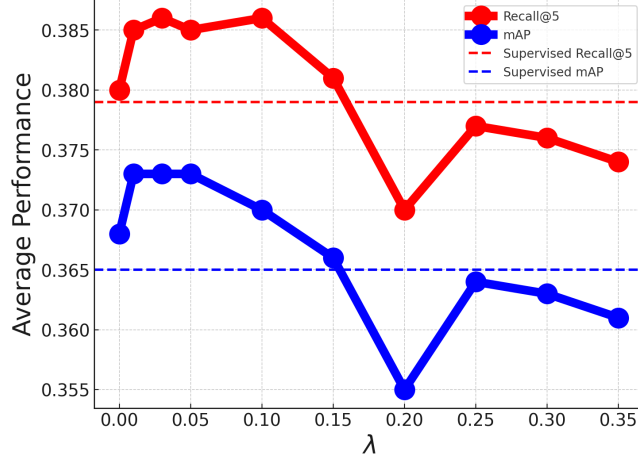


Figure 9. Average Recall@5 and mAP for different  $\lambda$ . A&D with the DINO alignment backbone trained on the object+style training set.

$$mAP = \frac{\sum_{i=1}^s AP_i}{s},$$

where  $AP_i$  is the average precision score for the  $i$ -th synthetic image, and  $s$  is the total number of synthetic images.

## D. Visualization of attribution results

As illustrated in Figure 10, all methods retrieve content-relevant images rather than merely matching based on color. For instance, in the “spider on a finger” example, the original background is blue, yet none of the top-10 matches from any method contain a blue background—highlighting that semantic cues (e.g., the spider) dominate over low-level color similarity. Although all approaches successfully retrieve the correct exemplar, A&D appears to rank more semantically aligned images higher, such as the second and ninth results showing a spider on a hand. In the “pot on a red desk” example, color does influence retrieval to some extent: red pots appear among the top matches. This is reasonable, as color can contribute to similarity. However, A&D strikes a better balance between semantic content and color, retrieving only two red pots, while the Supervised model retrieves four and even ranks a red pot as the top result.

## E. More Discussions

**Does Alignment Matter? Yes!** Figure 7 presents the Frobenius norms of the difference between the cross-domain covariance matrix and the identity matrix, computed for synthetic and exemplar features from AbC’s object-centric training set. The cross-domain covariance matrix converges towards the identity matrix as the alignment between domains improves. Therefore, a lower Frobenius norm directly correlates with better alignment. Our results reveal that MoCo, DINO, and ViT exhibit significantly lower F-norms, indicating superior alignment compared to CLIP and SSCD. This finding aligns with the performance outcomes of our A&D method, as detailed in Table 1. The choice of alignment backbone is crucial, as

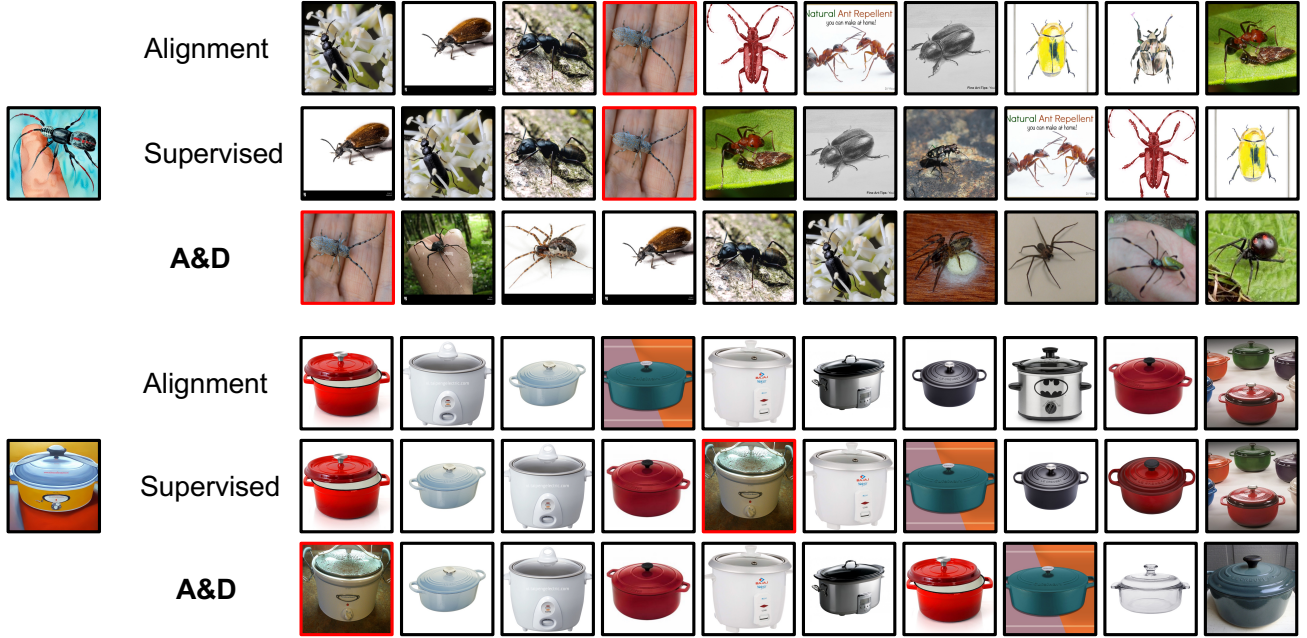


Figure 10. More attribution results visualization.

stronger backbones enable our A&D method to potentially surpass even supervised approaches in cross-domain alignment.

**Is Contrastive Alone Sufficient? No.** As demonstrated in Table 1, our framework using the ViT alignment backbone ranks third among all 20 cases in terms of average Recall@5 and mAP. This indicates that large-scale supervised pretraining also plays a significant role in enhancing alignment, complementing contrastive learning approaches.

**Combining A&D with other methods** In Table 3, we used DINO as the alignment backbone and combined our A&D method with both supervised learning and pseudo-labeling approaches. The results indicate that A&D does not consistently enhance its performance. For instance, while the combination of A&D with pseudo-labeling shows an average improvement in Recall@5 and mAP, it leads to a performance drop on the ImageNet-Seen test set and the ImageNet-Unseen set when prompted with Media. A similar trend is observed when combining A&D with the supervised method: although there is an improvement on the ImageNet-Seen and ImageNet-Unseen sets, there is a noticeable degradation in performance on the BAM-FG and Artchive datasets.

**Random initialization for  $\mathbf{H}_S$  and  $\mathbf{H}_E$**  We used identity initialization in our method and also experimented with random initialization. Specifically, we tried initializing the two linear mappings with both the same and different random matrices. In Table 5, we observe that when the two linear mappings are initialized with the same random matrix, the performance of our A&D method does not degrade significantly and remains comparable to the supervised method. However, when the mappings are initialized with different random matrices, our A&D method fails across all alignment backbones on all test sets. This is because identical initialization minimizes the likelihood of permutation occurring during ICA, thereby achieving alignment. Conversely, when initialized with different matrices, permutation almost certainly occurs, making alignment impossible.

**Effect of disentanglement** As illustrated in Figure 12, the features clearly becomes more uncorrelated after disentanglement.

## F. Regularization Details

**$\mathbf{H}_S^\top \mathbf{H}_E$  for regularization** We use  $\|\mathbf{H}_S^\top \mathbf{H}_E - \mathbf{I}\|_F$  as the regularizer. As shown in Table 5, it is slightly worse than the regularization in the main paper—except when DINO is used as the alignment backbone—yet remains comparable to the supervised method, supporting our theoretical analysis. Overall, when  $\mathbf{H}_S$  and  $\mathbf{H}_E$  are initialized as identity matrices, either

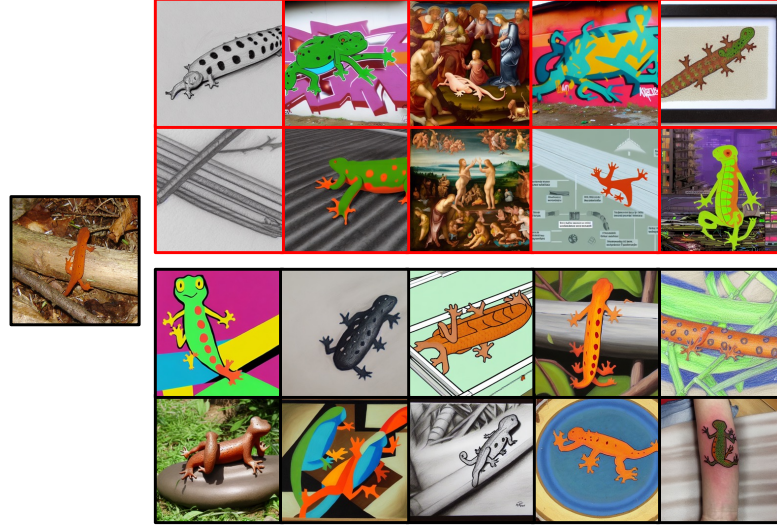


**Figure 11. Visualization of the object-centric training set in the AbC benchmark.** The image on the left shows a real exemplar, while the 20 images on the right illustrate a subset of its paired synthetic counterparts. In the AbC benchmark, the quality of synthetic data varies significantly. Some images, such as those outlined in black at the bottom, provide strong supervisory signals. In contrast, many others—such as those highlighted in red at the top—are noisy or ambiguous, potentially hindering effective training. These 20 examples represent only a small portion of the hundreds of synthetic images generated per exemplar and do not fully capture the overall variability and noise present in the dataset.

the self-orthogonality regularizers  $\|\mathbf{H}_S^\top \mathbf{H}_S - \mathbf{I}\|_F$  and  $\|\mathbf{H}_E^\top \mathbf{H}_E - \mathbf{I}\|_F$  or the cross-term regularizer  $\|\mathbf{H}_S^\top \mathbf{H}_E - \mathbf{I}\|_F$  alone is sufficient to preserve alignment.

**Regularization matters** As shown in Table 4, attribution performance degrades over time when regularization is not applied, whereas with regularization, performance remains stable. The reason why our A&D method still performs well in the early epochs without regularization is due to the identity initialization, which is an orthogonal matrix. Additionally, the initialization for the two linear mappings is identical, further preventing permutation at the beginning. However, as training progresses, the likelihood of permutation increases and the alignment breaks without regularization, leading to degradation in attribution performance.

**Appropriate values for the hyperparameter  $\lambda$**  We trained our A&D method using the DINO alignment backbone with different values of  $\lambda$ , which controls  $\mathcal{L}_{\text{Reg}}$ . Figure 9 shows the resulting attribution performance. For better comparison, we also include the performance of the supervised method as dashed lines. The graph indicates that both too low and too high values of  $\lambda$  are detrimental to A&D’s performance. A lower  $\lambda$  leads to degradation over time, as discussed earlier, while a higher  $\lambda$  restricts the mappings’ ability to make the features more independent. Empirically,  $\lambda$  should be chosen between 0.05 and 0.15 to balance performance and training stability.

## G. Full Experimental Results

In addition to using the object + style training set, we also conducted experiments on the object-centric training set and the style training set. The results are presented in Tables 6, 7, 8, 9. We also report Recall@10 and Recall@100 in these tables.

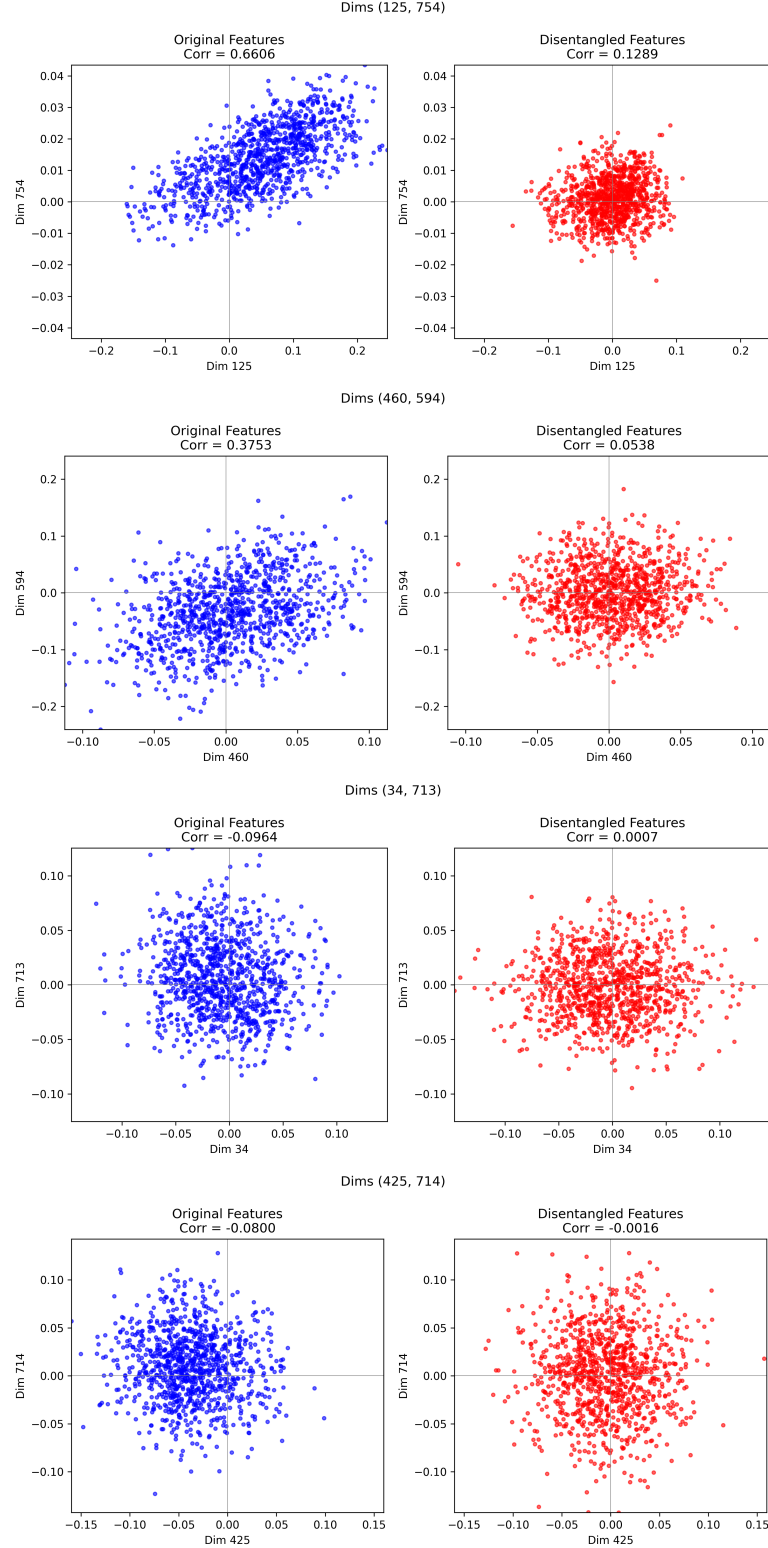


**Figure 12. Visualization of 1000 synthetic image features before and after disentanglement using DINO as the alignment backbone.** Each row corresponds to a randomly selected pair of feature dimensions. The left column shows the original features (alignment), while the right column shows the mapped (disentangled) features. We report the Pearson correlation coefficient for each pair, demonstrating how the disentanglement makes the feature dimensions uncorrelated.

Table 3. Performance of combining our A&D with Supervised training and Pseudo labeling. The models are trained on the object + style training set.

Source	ImageNet-Seen				BAM-FG				ImageNet-Unseen				Artchive				Average
	GPT		Media		GPT		Object		GPT		Media		GPT		Object		
$F_{\text{base}}$	Method	R@5	mAP	R@5	mAP	R@5	mAP	R@5	mAP	R@5	mAP	R@5	mAP	R@5	mAP	R@5	mAP
	Pretrain	0.433	0.393	0.288	0.255	0.148	0.163	0.193	0.219	0.831	0.795	0.540	0.492	0.183	0.181	0.140	0.136
	A&D	0.491	0.448	0.364	0.323	0.167	0.186	0.210	0.239	0.845	0.811	0.633	0.581	0.212	0.214	0.164	0.161
DINO	Pseudo	<b>0.471</b>	<b>0.426</b>	<b>0.374</b>	<b>0.330</b>	0.127	0.142	0.164	0.187	0.840	0.804	<b>0.639</b>	<b>0.588</b>	0.211	0.216	0.161	0.160
	A&D+Pse	0.466	0.424	0.352	0.311	<b>0.165</b>	<b>0.185</b>	<b>0.213</b>	<b>0.243</b>	<b>0.842</b>	<b>0.808</b>	0.608	0.559	<b>0.225</b>	<b>0.233</b>	<b>0.178</b>	<b>0.179</b>
	Superv	0.475	0.433	0.351	0.311	<b>0.165</b>	<b>0.184</b>	<b>0.212</b>	<b>0.239</b>	0.842	0.810	0.598	0.549	0.217	<b>0.221</b>	<b>0.170</b>	<b>0.169</b>
	A&D+Sup	<b>0.484</b>	<b>0.441</b>	<b>0.359</b>	<b>0.320</b>	0.147	0.158	0.190	0.211	<b>0.844</b>	<b>0.811</b>	<b>0.610</b>	<b>0.562</b>	0.191	0.194	0.150	0.149

Table 4. A&D with DINO alignment backbone trained without  $\lambda$ . The models are trained on the object + style training set. The table shows the performance degradation as the training progresses without  $\lambda$ .

Source	ImageNet-Seen				BAM-FG				ImageNet-Unseen				Artchive				Average
	GPT		Media		GPT		Object		GPT		Media		GPT		Object		
$\lambda$	Epochs	R@5	mAP	R@5	mAP	R@5	mAP	R@5	mAP	R@5	mAP	R@5	mAP	R@5	mAP	R@5	mAP
	No.10	0.482	0.446	0.340	0.309	0.159	0.177	0.211	0.240	0.856	0.825	0.624	0.579	0.204	0.205	0.162	0.159
	No.20	0.461	0.429	0.323	0.296	0.156	0.174	0.210	0.239	0.853	0.822	0.611	0.568	0.196	0.196	0.155	0.151
$\lambda = 0$	No.30	0.454	0.423	0.319	0.292	0.156	0.173	0.210	0.238	0.852	0.821	0.605	0.562	0.196	0.194	0.153	0.149
	No.40	0.452	0.421	0.317	0.290	0.155	0.172	0.209	0.237	0.851	0.820	0.604	0.561	0.195	0.192	0.153	0.148
	No.10	0.491	0.448	0.364	0.323	0.167	0.186	0.210	0.239	0.845	0.811	0.633	0.581	0.212	0.214	0.164	0.161
	No.20	0.491	0.447	0.358	0.320	0.166	0.184	0.210	0.239	0.846	0.812	0.634	0.581	0.211	0.212	0.164	0.160
$\lambda = 0.1$	No.30	0.491	0.447	0.358	0.320	0.164	0.182	0.209	0.238	0.847	0.814	0.634	0.582	0.210	0.209	0.162	0.159
	No.40	0.490	0.448	0.357	0.320	0.164	0.182	0.209	0.238	0.846	0.814	0.634	0.582	0.209	0.208	0.161	0.157

Table 5. Ablation results. Here, HSHE means the  $\mathcal{L}_{\text{Reg}}$  for A&D is calculated using  $\|\mathbf{H}_S^\top \mathbf{H}_E - \mathbf{I}\|_F$ . RandS means  $\mathbf{H}_S$  and  $\mathbf{H}_E$  are initialized as the same random matrix. RandD means  $\mathbf{H}_S$  and  $\mathbf{H}_E$  are initialized as different random matrices.

Source	ImageNet-Seen				BAM-FG				ImageNet-Unseen				Artchive				Average
	GPT		Media		GPT		Object		GPT		Media		GPT		Object		
$F_{\text{base}}$	Method	R@5	mAP	R@5	mAP	R@5	mAP	R@5	mAP	R@5	mAP	R@5	mAP	R@5	mAP	R@5	mAP
	Pretrain	0.390	0.347	0.239	0.211	0.130	0.144	0.187	0.211	0.761	0.717	0.460	0.408	0.169	0.164	0.131	0.125
	HSHE	0.437	0.393	0.293	0.260	0.150	0.168	0.210	0.240	0.797	0.758	0.529	0.479	0.201	0.201	0.159	0.158
MoCo	RandS	0.434	0.390	0.291	0.259	0.149	0.167	0.210	0.240	0.796	0.758	0.529	0.478	0.201	0.201	0.159	0.158
	RandD	-	-	-	-	-	-	-	-	-	-	-	-	-	-	-	-
	A&D	0.444	0.399	0.313	0.277	0.157	0.175	0.209	0.238	0.804	0.765	0.569	0.512	0.204	0.204	0.158	0.154
	Supervise	0.437	0.394	0.295	0.262	0.153	0.172	0.209	0.238	0.791	0.753	0.519	0.467	0.208	0.209	0.165	0.165
	Pretrain	0.433	0.393	0.288	0.255	0.148	0.163	0.193	0.219	0.831	0.795	0.540	0.492	0.183	0.181	0.140	0.136
	HSHE	0.501	0.459	0.361	0.325	0.164	0.184	0.213	0.246	0.852	0.820	0.626	0.578	0.217	0.221	0.171	0.170
DINO	RandS	0.494	0.454	0.354	0.318	0.164	0.182	0.214	0.245	0.851	0.818	0.622	0.573	0.215	0.218	0.169	0.168
	RandD	-	-	-	-	-	-	-	-	-	-	-	-	-	-	-	-
	A&D	0.491	0.448	0.364	0.323	0.167	0.186	0.210	0.239	0.845	0.811	0.633	0.581	0.212	0.214	0.164	0.161
	Supervise	0.475	0.433	0.351	0.311	0.165	0.184	0.212	0.239	0.842	0.810	0.598	0.549	0.217	0.221	0.170	0.169
	Pretrain	0.355	0.310	0.242	0.210	0.168	0.193	0.224	0.259	0.785	0.726	0.474	0.410	0.201	0.210	0.156	0.161
	HSHE	0.454	0.408	0.331	0.290	0.168	0.191	0.217	0.252	0.827	0.782	0.580	0.520	0.165	0.165	0.128	0.127
ViT	RandS	0.440	0.396	0.316	0.277	0.169	0.192	0.221	0.255	0.828	0.783	0.573	0.511	0.166	0.166	0.130	0.127
	RandD	-	-	-	-	-	-	-	-	-	-	-	-	-	-	-	-
	A&D	0.440	0.395	0.295	0.259	0.203	0.229	0.251	0.288	0.845	0.805	0.561	0.500	0.229	0.240	0.176	0.182
	Supervise	0.448	0.398	0.315	0.274	0.182	0.209	0.234	0.272	0.820	0.772	0.539	0.474	0.206	0.216	0.159	0.163

Table 6. Full evaluation results on ImageNet-Seen.

Source			ImageNet-Seen							
Prompts			GPT				Media			
$F_{\text{base}}$	Method	Dataset	R@5	R@10	R@100	mAP	R@5	R@10	R@100	mAP
MoCo	Pretrain	None	0.390	0.425	0.537	0.347	0.239	0.267	0.372	0.211
		Object	0.443	0.479	0.589	0.400	0.313	0.345	0.457	0.278
	Supervised	Style	0.409	0.442	0.555	0.365	0.263	0.292	0.400	0.232
		Object+Style	0.437	0.472	0.581	0.394	0.295	0.327	0.435	0.262
	Pseudo	Object	0.424	0.456	0.559	0.381	0.258	0.285	0.384	0.227
		Style	0.402	0.439	0.556	0.355	0.265	0.294	0.406	0.230
	A&D	Object+Style	0.418	0.452	0.556	0.377	0.251	0.279	0.375	0.221
		Object	0.447	0.477	0.577	0.404	0.310	0.340	0.445	0.276
	A&D	Style	0.422	0.457	0.579	0.377	0.299	0.334	0.465	0.264
		Object+Style	0.444	0.478	0.589	0.399	0.313	0.347	0.468	0.277
DINO	Pretrain	None	0.433	0.467	0.579	0.393	0.288	0.321	0.428	0.255
		Object	0.479	0.517	0.628	0.437	0.368	0.399	0.511	0.325
	Supervised	Style	0.443	0.476	0.590	0.402	0.315	0.348	0.461	0.278
		Object+Style	0.475	0.510	0.623	0.433	0.351	0.383	0.496	0.311
	Pseudo	Object	0.463	0.497	0.606	0.420	0.333	0.366	0.479	0.294
		Style	0.428	0.467	0.591	0.384	0.323	0.358	0.481	0.282
	A&D	Object+Style	0.471	0.509	0.625	0.426	0.374	0.408	0.527	0.330
		Object	0.493	0.524	0.620	0.450	0.354	0.384	0.484	0.317
	A&D	Style	0.452	0.488	0.607	0.411	0.348	0.382	0.509	0.306
		Object+Style	0.491	0.523	0.625	0.448	0.364	0.395	0.507	0.323
ViT	Pretrain	None	0.355	0.393	0.530	0.310	0.242	0.275	0.413	0.210
		Object	0.452	0.489	0.615	0.406	0.335	0.372	0.509	0.294
	Supervised	Style	0.357	0.396	0.539	0.314	0.253	0.290	0.432	0.219
		Object+Style	0.448	0.487	0.618	0.398	0.315	0.353	0.492	0.274
	Pseudo	Object	0.417	0.454	0.579	0.373	0.289	0.324	0.457	0.252
		Style	0.370	0.409	0.543	0.325	0.257	0.292	0.428	0.221
	A&D	Object+Style	0.361	0.400	0.539	0.319	0.266	0.305	0.447	0.230
		Object	0.440	0.476	0.596	0.394	0.314	0.354	0.487	0.275
	A&D	Style	0.387	0.425	0.566	0.342	0.269	0.306	0.461	0.233
		Object+Style	0.440	0.474	0.588	0.395	0.295	0.331	0.457	0.259
CLIP	Pretrain	None	0.236	0.277	0.437	0.195	0.137	0.160	0.274	0.118
		Object	0.350	0.397	0.561	0.298	0.293	0.336	0.503	0.249
	Supervised	Style	0.277	0.317	0.478	0.232	0.176	0.204	0.346	0.153
		Object+Style	0.329	0.376	0.540	0.280	0.222	0.258	0.428	0.190
	Pseudo	Object	0.110	0.139	0.273	0.087	0.071	0.090	0.192	0.058
		Style	0.100	0.121	0.230	0.082	0.036	0.043	0.080	0.030
	A&D	Object+Style	0.018	0.023	0.057	0.015	0.014	0.017	0.032	0.011
		Object	0.286	0.329	0.493	0.239	0.183	0.213	0.358	0.158
	A&D	Style	0.239	0.282	0.443	0.196	0.142	0.166	0.289	0.122
		Object+Style	0.257	0.300	0.468	0.212	0.153	0.177	0.304	0.132
SSCD	Pretrain	None	0.253	0.272	0.335	0.230	0.142	0.153	0.194	0.131
		Object	0.265	0.284	0.351	0.241	0.158	0.170	0.215	0.144
	Supervised	Style	0.254	0.273	0.339	0.228	0.144	0.155	0.199	0.132
		Object+Style	0.268	0.288	0.357	0.242	0.156	0.167	0.214	0.142
	Pseudo	Object	0.236	0.253	0.314	0.214	0.133	0.143	0.182	0.122
		Style	0.265	0.286	0.356	0.239	0.152	0.165	0.212	0.138
	A&D	Object+Style	0.267	0.289	0.360	0.241	0.154	0.167	0.215	0.140
		Object	0.262	0.281	0.345	0.237	0.147	0.159	0.201	0.135
	A&D	Style	0.259	0.279	0.343	0.233	0.146	0.158	0.201	0.134
		Object+Style	0.259	0.280	0.344	0.234	0.147	0.158	0.201	0.134

Table 7. Full evaluation results on BAM-FG.

Source			BAM-FG							
Prompts			GPT				Object			
$F_{\text{base}}$	Method	Dataset	R@5	R@10	R@100	mAP	R@5	R@10	R@100	mAP
MoCo	Pretrain	None	0.130	0.163	0.273	0.144	0.187	0.232	0.355	0.211
		Object	0.151	0.191	0.307	0.171	0.211	0.261	0.392	0.242
	Supervised	Style	0.150	0.188	0.303	0.168	0.207	0.255	0.381	0.235
		Object+Style	0.153	0.192	0.308	0.172	0.209	0.258	0.385	0.238
	Pseudo	Object	0.130	0.164	0.269	0.144	0.185	0.228	0.347	0.209
		Style	0.132	0.167	0.282	0.148	0.180	0.225	0.351	0.204
	A&D	Object+Style	0.132	0.166	0.273	0.146	0.187	0.232	0.351	0.212
		Object	0.146	0.183	0.292	0.163	0.206	0.256	0.382	0.235
	A&D	Style	0.157	0.194	0.301	0.174	0.206	0.254	0.371	0.235
		Object+Style	0.157	0.195	0.302	0.175	0.209	0.257	0.377	0.238
DINO	Pretrain	None	0.148	0.184	0.293	0.163	0.193	0.239	0.360	0.219
		Object	0.168	0.208	0.324	0.188	0.216	0.267	0.391	0.247
	Supervised	Style	0.164	0.204	0.318	0.183	0.210	0.257	0.381	0.237
		Object+Style	0.165	0.205	0.320	0.184	0.212	0.259	0.383	0.239
	Pseudo	Object	0.141	0.176	0.283	0.156	0.183	0.226	0.345	0.207
		Style	0.131	0.164	0.268	0.144	0.173	0.212	0.331	0.194
	A&D	Object+Style	0.127	0.159	0.259	0.142	0.164	0.204	0.324	0.187
		Object	0.161	0.200	0.312	0.180	0.212	0.261	0.387	0.242
	A&D	Style	0.164	0.204	0.309	0.184	0.205	0.253	0.369	0.234
		Object+Style	0.167	0.206	0.311	0.186	0.210	0.259	0.376	0.239
ViT	Pretrain	None	0.433	0.467	0.579	0.393	0.288	0.321	0.428	0.255
		Object	0.172	0.218	0.342	0.196	0.221	0.274	0.405	0.256
	Supervised	Style	0.182	0.230	0.359	0.209	0.231	0.288	0.425	0.270
		Object+Style	0.182	0.230	0.358	0.209	0.234	0.291	0.428	0.272
	Pseudo	Object	0.154	0.195	0.318	0.174	0.207	0.259	0.391	0.239
		Style	0.163	0.208	0.334	0.186	0.219	0.273	0.408	0.254
	A&D	Object+Style	0.103	0.132	0.227	0.117	0.141	0.178	0.287	0.162
		Object	0.167	0.212	0.336	0.190	0.219	0.272	0.404	0.253
	A&D	Style	0.187	0.232	0.343	0.213	0.227	0.278	0.392	0.261
		Object+Style	0.203	0.249	0.355	0.229	0.251	0.305	0.418	0.288
CLIP	Pretrain	None	0.129	0.170	0.310	0.148	0.174	0.225	0.374	0.200
		Object	0.166	0.218	0.364	0.195	0.216	0.275	0.431	0.252
	Supervised	Style	0.185	0.242	0.405	0.218	0.235	0.302	0.472	0.278
		Object+Style	0.186	0.243	0.408	0.219	0.236	0.303	0.474	0.278
	Pseudo	Object	0.070	0.097	0.216	0.084	0.098	0.129	0.256	0.115
		Style	0.012	0.017	0.049	0.014	0.018	0.025	0.066	0.021
	A&D	Object+Style	0.022	0.031	0.079	0.026	0.032	0.042	0.102	0.036
		Object	0.150	0.198	0.346	0.175	0.196	0.251	0.407	0.226
	A&D	Style	0.162	0.214	0.365	0.189	0.205	0.263	0.417	0.238
		Object+Style	0.173	0.226	0.380	0.202	0.216	0.276	0.431	0.251
SSCD	Pretrain	None	0.117	0.146	0.231	0.128	0.175	0.214	0.313	0.194
		Object	0.113	0.141	0.222	0.123	0.169	0.207	0.302	0.187
	Supervised	Style	0.119	0.148	0.234	0.130	0.174	0.215	0.315	0.193
		Object+Style	0.118	0.147	0.231	0.128	0.174	0.213	0.314	0.193
	Pseudo	Object	0.110	0.137	0.218	0.120	0.164	0.202	0.300	0.183
		Style	0.117	0.147	0.231	0.127	0.170	0.209	0.309	0.188
	A&D	Object+Style	0.110	0.137	0.216	0.118	0.161	0.198	0.292	0.178
		Object	0.120	0.149	0.234	0.130	0.177	0.216	0.317	0.197
	A&D	Style	0.118	0.148	0.232	0.129	0.175	0.215	0.314	0.195
		Object+Style	0.119	0.148	0.233	0.130	0.176	0.215	0.315	0.196

Table 8. Full evaluation results on ImageNet-Unseen.

Source			ImageNet-Unseen							
Prompts			GPT				Media			
$F_{\text{base}}$	Method	Dataset	R@5	R@10	R@100	mAP	R@5	R@10	R@100	mAP
MoCo	Pretrain	None	0.761	0.786	0.852	0.717	0.460	0.493	0.586	0.408
		Object	0.792	0.813	0.874	0.753	0.542	0.573	0.658	0.490
	Supervised	Style	0.783	0.806	0.868	0.742	0.493	0.526	0.612	0.443
		Object+Style	0.791	0.813	0.874	0.753	0.519	0.551	0.636	0.467
	Pseudo	Object	0.781	0.805	0.864	0.741	0.461	0.494	0.573	0.411
		Style	0.775	0.801	0.865	0.724	0.487	0.520	0.602	0.426
	A&D	Object+Style	0.778	0.802	0.862	0.736	0.452	0.483	0.563	0.402
		Object	0.807	0.828	0.881	0.769	0.552	0.584	0.673	0.501
	A&D	Style	0.793	0.818	0.879	0.754	0.561	0.601	0.710	0.502
		Object+Style	0.804	0.827	0.882	0.765	0.569	0.606	0.709	0.512
DINO	Pretrain	None	0.831	0.851	0.900	0.795	0.540	0.572	0.661	0.492
		Object	0.842	0.861	0.909	0.809	0.622	0.654	0.738	0.574
	Supervised	Style	0.838	0.858	0.905	0.803	0.576	0.608	0.698	0.526
		Object+Style	0.842	0.861	0.908	0.810	0.598	0.629	0.714	0.549
	Pseudo	Object	0.838	0.857	0.904	0.804	0.583	0.617	0.705	0.533
		Style	0.816	0.840	0.898	0.771	0.604	0.642	0.738	0.545
	A&D	Object+Style	0.840	0.860	0.912	0.804	0.639	0.672	0.761	0.588
		Object	0.849	0.866	0.907	0.816	0.622	0.652	0.734	0.573
	A&D	Style	0.837	0.856	0.906	0.801	0.627	0.664	0.761	0.572
		Object+Style	0.845	0.863	0.907	0.811	0.633	0.667	0.758	0.581
ViT	Pretrain	None	0.785	0.821	0.898	0.726	0.474	0.528	0.689	0.410
		Object	0.818	0.844	0.908	0.773	0.567	0.615	0.749	0.505
	Supervised	Style	0.785	0.820	0.898	0.727	0.479	0.534	0.700	0.415
		Object+Style	0.820	0.847	0.912	0.772	0.539	0.590	0.737	0.474
	Pseudo	Object	0.808	0.836	0.903	0.759	0.515	0.565	0.712	0.452
		Style	0.773	0.810	0.892	0.712	0.470	0.527	0.691	0.407
	A&D	Object+Style	0.794	0.827	0.902	0.737	0.525	0.580	0.739	0.457
		Object	0.828	0.851	0.910	0.781	0.571	0.616	0.746	0.509
	A&D	Style	0.814	0.842	0.906	0.762	0.525	0.577	0.742	0.460
		Object+Style	0.845	0.867	0.916	0.805	0.561	0.607	0.742	0.500
CLIP	Pretrain	None	0.580	0.644	0.818	0.500	0.239	0.285	0.472	0.201
		Object	0.710	0.754	0.868	0.645	0.511	0.567	0.733	0.447
	Supervised	Style	0.664	0.716	0.853	0.587	0.327	0.378	0.567	0.279
		Object+Style	0.701	0.745	0.864	0.633	0.389	0.445	0.628	0.332
	Pseudo	Object	0.313	0.371	0.580	0.248	0.142	0.174	0.331	0.115
		Style	0.317	0.371	0.585	0.259	0.079	0.093	0.163	0.064
	A&D	Object+Style	0.032	0.042	0.115	0.027	0.009	0.011	0.032	0.007
		Object	0.655	0.709	0.849	0.579	0.337	0.393	0.590	0.284
	A&D	Style	0.583	0.648	0.820	0.499	0.244	0.291	0.477	0.206
		Object+Style	0.607	0.672	0.833	0.525	0.258	0.305	0.486	0.218
SSCD	Pretrain	None	0.601	0.627	0.698	0.566	0.264	0.281	0.342	0.245
		Object	0.622	0.644	0.713	0.588	0.285	0.302	0.366	0.264
	Supervised	Style	0.599	0.623	0.699	0.565	0.267	0.285	0.347	0.247
		Object+Style	0.621	0.644	0.714	0.586	0.282	0.298	0.362	0.261
	Pseudo	Object	0.589	0.613	0.688	0.552	0.258	0.273	0.334	0.238
		Style	0.619	0.643	0.717	0.581	0.283	0.301	0.371	0.260
	A&D	Object+Style	0.618	0.642	0.717	0.581	0.285	0.304	0.374	0.263
		Object	0.614	0.637	0.708	0.576	0.273	0.289	0.353	0.252
	A&D	Style	0.609	0.633	0.706	0.572	0.272	0.288	0.352	0.250
		Object+Style	0.610	0.634	0.707	0.573	0.272	0.289	0.353	0.251

Table 9. Full evaluation results on Artchive.

Source			Artchive							
Prompts			GPT				Object			
$F_{\text{base}}$	Method	Dataset	R@5	R@10	R@100	mAP	R@5	R@10	R@100	mAP
MoCo	Pretrain	None	0.169	0.198	0.314	0.164	0.131	0.152	0.246	0.125
		Object	0.215	0.250	0.387	0.218	0.172	0.201	0.312	0.172
	Supervised	Style	0.204	0.237	0.371	0.204	0.160	0.188	0.297	0.160
		Object+Style	0.208	0.242	0.377	0.209	0.165	0.193	0.304	0.165
	Pseudo	Object	0.162	0.189	0.297	0.158	0.130	0.149	0.233	0.125
		Style	0.201	0.239	0.377	0.204	0.163	0.190	0.304	0.162
	A&D	Object+Style	0.166	0.192	0.304	0.162	0.132	0.153	0.241	0.128
		Object	0.195	0.224	0.332	0.193	0.153	0.173	0.264	0.150
	A&D	Style	0.205	0.234	0.339	0.204	0.155	0.177	0.262	0.152
		Object+Style	0.204	0.234	0.339	0.204	0.158	0.180	0.264	0.154
DINO	Pretrain	None	0.183	0.211	0.320	0.181	0.140	0.162	0.250	0.136
		Object	0.225	0.260	0.386	0.232	0.175	0.203	0.303	0.176
	Supervised	Style	0.214	0.247	0.374	0.221	0.168	0.193	0.293	0.168
		Object+Style	0.217	0.248	0.374	0.221	0.170	0.194	0.294	0.169
	Pseudo	Object	0.178	0.202	0.302	0.178	0.135	0.154	0.233	0.132
		Style	0.157	0.180	0.271	0.154	0.119	0.135	0.207	0.114
	A&D	Object+Style	0.211	0.245	0.375	0.216	0.161	0.187	0.297	0.160
		Object	0.218	0.249	0.365	0.222	0.171	0.196	0.293	0.171
	A&D	Style	0.213	0.239	0.344	0.214	0.158	0.178	0.260	0.156
		Object+Style	0.212	0.240	0.344	0.214	0.164	0.184	0.267	0.161
ViT	Pretrain	None	0.201	0.238	0.395	0.210	0.156	0.184	0.309	0.161
		Object	0.192	0.226	0.368	0.200	0.146	0.171	0.278	0.148
	Supervised	Style	0.208	0.245	0.400	0.218	0.159	0.187	0.310	0.164
		Object+Style	0.206	0.244	0.398	0.216	0.159	0.187	0.308	0.163
	Pseudo	Object	0.157	0.184	0.305	0.156	0.128	0.151	0.250	0.126
		Style	0.185	0.217	0.361	0.190	0.151	0.176	0.294	0.153
	A&D	Object+Style	0.156	0.191	0.349	0.161	0.115	0.139	0.257	0.114
		Object	0.165	0.193	0.305	0.165	0.129	0.150	0.237	0.127
	A&D	Style	0.214	0.247	0.380	0.226	0.161	0.185	0.280	0.166
		Object+Style	0.229	0.264	0.390	0.240	0.176	0.202	0.299	0.182
CLIP	Pretrain	None	0.186	0.234	0.440	0.198	0.140	0.175	0.335	0.144
		Object	0.249	0.305	0.512	0.282	0.188	0.231	0.396	0.207
	Supervised	Style	0.264	0.325	0.565	0.307	0.203	0.251	0.447	0.228
		Object+Style	0.259	0.317	0.550	0.297	0.201	0.247	0.437	0.223
	Pseudo	Object	0.155	0.203	0.416	0.178	0.115	0.150	0.314	0.126
		Style	0.162	0.209	0.428	0.185	0.123	0.157	0.330	0.134
	A&D	Object+Style	0.185	0.238	0.489	0.212	0.147	0.189	0.391	0.161
		Object	0.214	0.267	0.481	0.235	0.163	0.203	0.372	0.173
	A&D	Style	0.207	0.256	0.463	0.225	0.156	0.194	0.352	0.165
		Object+Style	0.229	0.282	0.500	0.256	0.176	0.218	0.387	0.190
SSCD	Pretrain	None	0.151	0.171	0.241	0.142	0.123	0.140	0.203	0.115
		Object	0.159	0.179	0.255	0.151	0.133	0.149	0.215	0.125
	Supervised	Style	0.154	0.173	0.246	0.144	0.126	0.142	0.207	0.118
		Object+Style	0.159	0.179	0.254	0.150	0.131	0.148	0.213	0.123
	Pseudo	Object	0.141	0.159	0.226	0.132	0.115	0.131	0.191	0.107
		Style	0.160	0.183	0.264	0.151	0.130	0.148	0.218	0.121
	A&D	Object+Style	0.156	0.177	0.255	0.147	0.126	0.143	0.210	0.119
		Object	0.154	0.173	0.246	0.145	0.125	0.141	0.205	0.117
	A&D	Style	0.150	0.169	0.239	0.141	0.122	0.138	0.201	0.114
		Object+Style	0.150	0.170	0.241	0.142	0.123	0.139	0.202	0.115